

Mitigating barren plateaus of variational quantum eigensolvers

Xia Liu,¹ Geng Liu,¹ Jiaxin Huang,¹ Hao-Kai Zhang,^{1,2} and Xin Wang^{1,*}

¹Institute for Quantum Computing, Baidu Research, Beijing 100193, China

²Institute for Advanced Study, Tsinghua University, Beijing 100084, China

(Dated: August 15, 2022)

Variational quantum algorithms (VQAs) are expected to establish valuable applications on near-term quantum computers. However, recent works have pointed out that the performance of VQAs greatly relies on the expressibility of the ansatzes and is seriously limited by optimization issues such as barren plateaus (i.e., vanishing gradients). This work proposes the state efficient ansatz (SEA) for accurate ground state preparation with improved trainability. We show that the SEA can generate an arbitrary pure state with much fewer parameters than a universal ansatz, making it efficient for tasks like ground state estimation. Then, we prove that barren plateaus can be efficiently mitigated by the SEA and the trainability can be further improved most quadratically by flexibly adjusting the entangling capability of the SEA. Finally, we investigate a plethora of examples in ground state estimation where we obtain significant improvements in the magnitude of cost gradient and the convergence speed.

Introduction.— Quantum computers are expected to achieve quantum advantages [1] in solving valuable problems [2–5]. Before arriving at universal quantum computing, a key direction is to explore the power of noisy intermediate-scale quantum (NISQ) [6] devices in important fields such as quantum chemistry [7, 8] and quantum machine learning [9–13]. Recent results [14–19] have shown that quantum advantages in specific tasks can be achieved using such devices.

One common paradigm for designing quantum solutions using NISQ devices is variational quantum algorithms (VQAs) [20–22]. VQAs are promising to deliver applications in many important topics, including ground state preparation [7, 8, 23], quantum data compression [24, 25], machine learning [9, 26–30], and combinatorial optimization [31, 32]. Combining the advantages of classical computers and quantum devices, VQAs adopt parameterized quantum circuits (PQCs, also known as ansatzes) [33] and utilize classical computers to optimize the parameters to minimize the cost functions that are designed for solving target problems.

Among the numerous VQAs, the variational quantum eigensolver (VQE) for ground state estimation is a central one of both practical and theoretical interests. For VQE, one common approach is to utilize fixed structure ansatzes, such as the hardware-efficient ansatz [34] and the unitary coupled cluster ansatz [8, 35, 36], which require a large depth to achieve high accuracy when the problem scale is large. On the other hand, there are adaptive structure ansatzes [37–41], which usually suffer from relatively high costs of both quantum and classical resources.

Despite the success of VQE, expressibility [42–44] and trainability [45–47] are still two critical challenges of designing ansatzes for it. To improve the accuracy of the algorithms, deep ansatzes are usually preferred for their strong expressibility. This could be seen in the same spirit of deep neural networks in machine learning. However, recent works [44, 48, 49] imply that strong expressibility will lead to poor trainability due to the barren plateau phenomenon [45, 50, 51], i.e.,

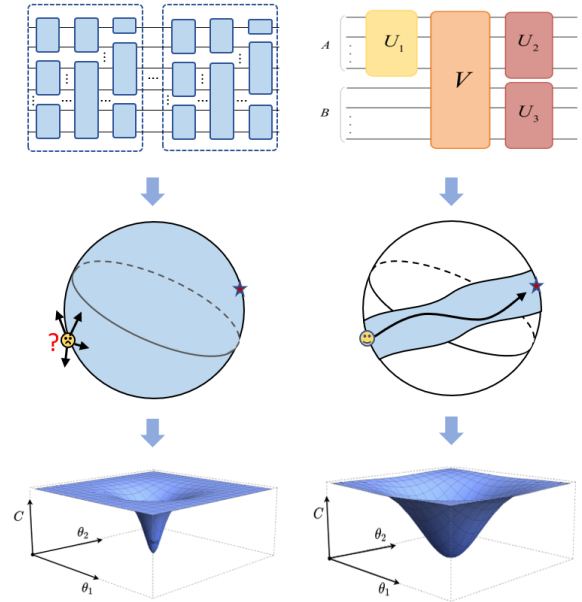


FIG. 1. **Illustration of our main result.** The left column demonstrates the difficulty in the optimization process of general ansatzes, which have high expressibility. The optimization process of State Efficient Ansatz (SEA) is depicted in the right column, with its conceptual framework represented in the upper right, where A and B are two subsystems. Schmidt coefficient layer U_1 , entangling layer V , and local basis changing layer U_2, U_3 , are the three parts of SEA. The key feature of SEA is reducing the optional range of paths, leading to a more favorable landscape, as shown at the bottom.

exponentially vanishing gradients in training with respect to the number of qubits. This technical bottleneck seriously restricts the scalability of VQE. Despite a plethora of recent attempts to address the barren plateaus through adjusting initialization [52, 53], cost functions [54, 55], and architectures [56], there is still a strong need for extending the scalability of VQE by improving the trainability while preserving the effectiveness.

* wangxin73@baidu.com

To overcome these challenges, we propose the State Efficient Ansatz (SEA), as shown in Fig. 1. By removing the redundancy between the sets of universal unitary and universal pure quantum state, SEA can represent an arbitrary pure quantum state with fewer parameters, resulting in its efficiency in all the tasks that are essentially learning a quantum state, which we call the state-oriented tasks (such as VQE). Moreover, by adjusting the number of CNOT gates in the entangling layer (see Fig. 2), SEA has the ability to learn a target ground state with low bipartite entanglement, where we proved that barren plateaus can be effectively mitigated by the SEA. To be specific, the SEA can effectively enhance the gradient magnitude up to a square root of the scaling of the global 2-design case. We further investigate a plethora of examples in ground state estimation through numerical experiments and establish evident improvements in both the overall behavior and the magnitude of the cost gradient .

State Efficient Ansatz.— The intuition of SEA is to prune the redundant expressibility of an ansatz in the state-oriented tasks by utilizing the Schmidt representation [57] of pure states, which also inspires the tree tensor network [58–61]. Specifically, the input system has two subsystems A and B , and the ansatz comprises three parts. The first part is the *Schmidt coefficient layer* U_1 acting on subsystem A . The second part is the *entangling layer* V acting on the whole system AB to create entanglement between two subsystems. The last part is the *local basis changing layer (LBC layer)*, which consists of two local circuits, U_2 and U_3 , applied to the two subsystems respectively. The whole structure of SEA is shown in the upper right of Fig. 1 and can be written as

$$S(\boldsymbol{\theta}) \equiv (U_2(\boldsymbol{\theta}_2) \otimes U_3(\boldsymbol{\theta}_3))V(U_1(\boldsymbol{\theta}_1) \otimes I), \quad (1)$$

where S is the unitary representation of SEA, $\boldsymbol{\theta} = \{\boldsymbol{\theta}_1, \boldsymbol{\theta}_2, \boldsymbol{\theta}_3\}$, and each $\boldsymbol{\theta}_i (i = 1, 2, 3)$ is a parameter vector.

Now we explain how SEA reduces redundant expressibility from the perspective of degrees of freedom (DOF). For state-oriented tasks, the DOF of the $2N$ -qubit pure state set is $2^{2N+1} - 2$ and the DOF of the unitary group $\mathcal{U}(2^{2N})$ is 4^{2N} [62]. Therefore, using a universal $2N$ -qubit PQC that can represent a universal unitary set to generate a universal pure states set is overkill. In contrast, SEA has a quadratic advantage in the parametric DOF compared to universal PQCs. Note that a universal N -qubit PQC U_i has $O(4^N)$ DOF [63]. Therefore, a $2N$ -qubit SEA with universal $U_i (i = 1, 2, 3)$ also has $O(4^N)$ parametric DOF. In comparison, a $2N$ -qubit universal PQC has $O(4^{2N})$ parametric DOF. Therefore, SEA requires quadratically fewer parameters than a general PQC of the same dimension while retaining the ability to generate an arbitrary pure state. It is also worth pointing out that SEA can reach the optimal DOF to generate pure states set, which is the $2 \times 4^N - 2$, by removing the redundant freedom in U_1, U_2, U_3 . In this sense, we call it *state efficient ansatz*.

After clarifying that SEA is efficient in generating an arbitrary pure state, we here elaborate the effectiveness of SEA. For simplicity, we assume both subsystems A and B have N qubits and let $|0\rangle^{\otimes 2N}$ be an initial state sent into SEA. An example of SEA is shown in Fig. 2. To be specific, U_1 is the Schmidt coefficient layer with $U_1|0\rangle^{\otimes N} = \sum_{k=0}^{2^N-1} \lambda_k |k\rangle_A$,

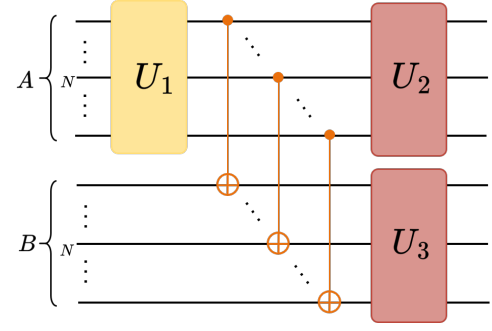


FIG. 2. **An established case of SEA.** Schmidt coefficient layer U_1 has universal wavefunction expressibility. The entangling layer consists of N CNOTs, and the LBC layer comprises two local universal PQCs, U_2 and U_3 . The evolution of $|0\rangle^{\otimes 2N}$ under this SEA is as follows. After Schmidt coefficient layer, we obtain $\sum_{k=0}^{2^N-1} \lambda_k |k\rangle_A |0\rangle^{\otimes N}$. Then we get $\sum_{k=0}^{2^N-1} \lambda_k |k\rangle_A |k\rangle_B$ after implementing N CNOTs. Finally, we obtain the output state $\sum_{k=0}^{2^N-1} \lambda_k |v_k\rangle_A |v_k\rangle_B$ after the LBC layer.

where $\{|k\rangle\}_{k=0}^{2^N-1}$ is the computational basis. At the entangling layer, we set a composition of N CNOTs controlled and targeted on the qubit-pairs $\{(i, N+i)\}_{i=0}^{N-1}$. At the last layer, we apply U_2 and U_3 on subsystems A and B , respectively, such that $U_2|k\rangle_A = |v_k\rangle_A$ and $U_3|k\rangle_B = |v_k\rangle_B$. Then after SEA, $|0\rangle^{\otimes 2N}$ will evolve into $\sum_{k=0}^{2^N-1} \lambda_k |v_k\rangle_A |v_k\rangle_B$. Note that this exactly forms a Schmidt decomposition with tunable Schmidt coefficients and bases. Since any pure state has a form of Schmidt decomposition, SEA can evolve an initial state $|0\rangle^{\otimes 2N}$ into an arbitrary $2N$ -qubit pure state if U_1 can generate an arbitrary N -qubit pure state (that is, U_1 possessing *universal wavefunction expressibility*) and U_2, U_3 are universal. The whole process of SEA acting on the initial state $|0\rangle^{\otimes 2N}$ is shown in Fig. 2.

The above analysis implies that SEA with a U_1 of the universal wavefunction expressibility and U_2, U_3 being universal can accurately solve state-oriented tasks. Note that an N -qubit SEA has the universal wavefunction expressibility under the same conditions, so we can use it as the Schmidt coefficient layer of a $2N$ -qubit SEA to generate an arbitrary $2N$ -qubit pure state.

According to SEA's ability to evolve $|0\rangle^{\otimes 2N}$ into an arbitrary $2N$ -qubit pure state, we can conclude that SEA is effective for the VQE, which aims to variationally find the ground state of a given Hamiltonian. To be specific, for any $2N$ -qubit Hamiltonian H , the goal of the VQE is to find the ground state energy $E_0 = \min_{|\psi\rangle} \langle \psi | H | \psi \rangle$, where the minimization is over the $2N$ -qubit pure state set. Since a $2N$ -qubit SEA could generate an arbitrary pure state, it can obtain E_0 of a Hamiltonian after the optimization. This exactly illustrates the effectiveness of SEA when used in VQE. More details can be found in Sec. II of the Supplemental Material.

When dealing with a specific task, we can further optimize SEA if we know certain information about the entanglement of the target quantum state. The SEA mentioned before can generate a pure state with full Schmidt rank. However, if the

target quantum state is weakly entangled, we can change the structure of the entangling layer to reduce the cost without sacrificing performance. The effectiveness of SEA, in this case, is described in the following proposition.

Proposition 1 *If U_1 can generate any N -qubit pure state that is a superposition of at most K computational basis states, then for any $|\phi\rangle$, there exists an SEA output state $|\psi\rangle$ with $F(|\phi\rangle, |\psi\rangle) \geq \min\{\frac{K}{r}, 1\}$, where $F(|\phi\rangle, |\psi\rangle)$ is the fidelity between $|\phi\rangle$ and $|\psi\rangle$, and r is the Schmidt rank of $|\phi\rangle$.*

We can tune the value K in Proposition 1, which corresponds to the entangling capability, by adjusting the number of CNOT gates in the entangling layer. This proposition guarantees that SEA with fewer CNOT gates still has a strong expressibility for learning weakly entangled quantum states. More experiments are shown in *Numerical Simulation of Experiments*.

So far, our analysis of SEA's effectiveness assumes perfect training. However, in practice, trainability is also an important factor to be considered. Many common ansatzes suffer from the notorious barren plateaus phenomenon [45]. It was shown that the cost gradient vanishes exponentially in the number of qubits for a randomly initialized PQC with sufficient depth, if the unitary ensemble generated by the PQC is sufficiently random to accord with the Haar distribution over the unitary group up to the second moment, i.e., forming a unitary 2-design. The following proposition implies that SEA does not form a unitary 2-design even if it has enough expressibility for state-oriented tasks.

Proposition 2 *SEA with $U_i (i = 1, 2, 3)$ being local 2-design and $\widetilde{\text{CNOT}}$ as entangling layer does not form a 2-design on the global system.*

As we have known that a large class of random PQCs will end up forming a 2-design when the depth is large [45] and this is the usual case in VQAs, Proposition 2 implies that even though the local structures of SEA have strong expressibility by forming 2-designs, SEA will still not form a global 2-design. Thus SEA could avoid the known definite zone of barren plateaus without losing effectiveness on VQE. Moreover, SEA will maintain this property even if we change the number of CNOTs in the entangling layer. In fact, with less expressibility, SEA will be farther from being a 2-design. The proof can be found in Sec. IV of the Supplemental Material.

However, not being a unitary 2-design does not guarantee good trainability. In the following, we conduct a more rigorous analysis of SEA's trainability.

Mitigating Barren Plateaus.— In this section we estimate the trainability and expressibility of the SEA by computing the variance of the cost gradient [45, 54] and the frame potential [48], respectively, given that the sub-blocks in the SEA are sampled from local unitary 2-design ensembles. We show that by tuning the number of CNOT gates in the entangling layer, the SEA could continuously change the entanglement of the prepared state, and hence flexibly balance the trade-off between trainability and expressibility [44]. Especially, if the target state is weakly entangled, the SEA could gain a square

root advantage over the common circuit ansatzes such as the hardware-efficient ansatz, etc.

Trainability is one of the most concerning problems in VQAs. If the adopted ansatz forms a unitary 2-design, the optimization process will be crippled due to the exponentially vanishing gradients, resulting in a severe issue on the trainability of VQAs. Specifically, we consider the VQE cost function $C(\boldsymbol{\theta})$ with an initial state $|0\rangle^{\otimes 2N}$, an objective operator H and a circuit ansatz $\mathbf{U}(\boldsymbol{\theta})$ on $2N$ qubits and the gradient component $\partial_\mu C = \frac{\partial C}{\partial \theta_\mu}$ with respect to the variational parameter θ_μ . Here we assume that all sub-blocks with variational parameters in the SEA, i.e. U_1, U_2 , and U_3 , are sampled from local unitary 2-designs so that we can integrate them using the Weingarten calculus [64, 65]. Note that if θ_μ locates at U_i , we assume that the two parts in U_i are split by the gate corresponding to θ_μ (like in Fig. 8) are both local 2-designs. The trainability of the SEA under the above assumption is described by the following proposition, the proof of which is presented in Sec. V of the Supplemental Material.

Proposition 3 *For an SEA defined on $2N$ qubits with all sub-blocks being local 2-designs, the variance of the cost gradient scales with the number of qubits as*

$$\text{Var}_{\text{SEA}}[\partial_\mu C] \in \mathcal{O}(2^{-(N+M)}), \quad (2)$$

where $M \in \{0, 1, \dots, N\}$ denotes the number of CNOT gates used in the entangling layer and the variance is taken over all SEA sub-blocks independently.

This result notably implies that, by tuning the number of CNOT gates in the entangling layer, the SEA can effectively enhance the gradient magnitude up to a square root of the scaling of the global 2-design case $\text{Var}_{\text{Haar}}[\partial_\mu C] \in \mathcal{O}(2^{-2N})$, which is verified by the numerical results in Fig. 7 and Fig. 9. This is achieved by sacrificing the ability of expressing the highly entangled states since the number of CNOT gates determines the upper bound to the Schmidt rank of the prepared state. In other words, if the target state is actually low-entangled, e.g., the Schmidt rank does not scale or scales slowly with the number of qubits, the SEA could effectively mitigate barren plateaus and at the same time keep the capability of expressing the target state. For the VQE focusing on the ground state preparation task, this low-entanglement assumption is reasonable and supported by the entanglement area law for the ground states of gapped systems and the logarithmic growth for the ground states of gapless systems, at least in the 1-dimensional case [66].

The trade-off between the trainability and the expressibility [44] motivates us to further quantitatively analyze the expressibility of SEA using the t -degree frame potential [48], which is defined by

$$\mathcal{F}^{(t)} = \mathbb{E} \left[|\langle 0 | \mathbf{U}^\dagger \mathbf{V} | 0 \rangle|^{2t} \right], \quad (3)$$

where $|0\rangle$ denotes the zero state of the whole system and the expectation with respect to \mathbf{U}, \mathbf{V} is taken over two copies of the ansatz ensemble independently. The t -degree frame potential measures the expressibility of the ansatz ensemble up to

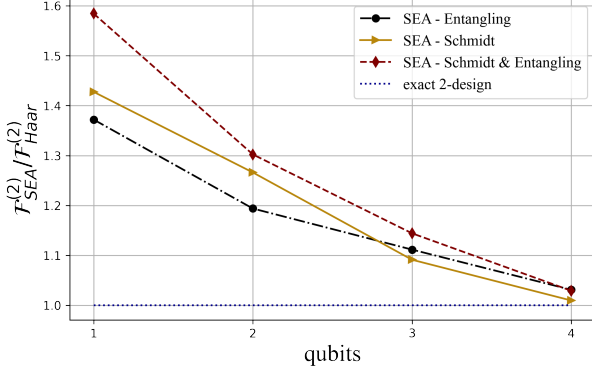


FIG. 3. **Second frame potentials of 8-qubit SEA with different Schmidt coefficient layers and entangling layers.** Yellow triangles, black dots, and red diamonds represent the frame potentials of 8-qubit SEA that change the number of qubits used in the Schmidt coefficient layer, entangling layer, and both two layers, respectively. Blue dotted line represents the frame potential of an exactly 2-design circuit. Each value is estimated using an ensemble of 5000 unitaries.

the t -th moment. It is known that the Haar random ensemble achieves the minimum frame potential $\mathcal{F}_{\text{Haar}}^{(t)}$ for each t , and this value can be achieved if and only if the ansatz ensemble is a t -design ensemble [67]. In addition, a smaller frame potential implies a stronger expressibility. Under the assumption of local 2-designs, we have the following proposition for the expressibility of the SEA. The proof can be found in Sec. VI of the Supplemental Material.

Proposition 4 *For an SEA defined on $2N$ qubits with all subblocks being local 2-designs, the first and second frame potential satisfies*

$$\mathcal{F}_{\text{SEA}}^{(1)} = 2^{-2N}, \quad (4)$$

$$\mathcal{F}_{\text{SEA}}^{(2)} \in \mathcal{O}(2^{-4N}). \quad (5)$$

The first frame potential of the SEA is identical to that of a global state 1-design $\mathcal{F}_{\text{Haar}}^{(1)} = 2^{-2N}$ and the second frame potential is in the same scaling with that of a global 2-design $\mathcal{F}_{\text{Haar}}^{(2)} = 2^{1-2N} (2^{-2N} + 1)$, in spite that the exact value of $\mathcal{F}_{\text{SEA}}^{(2)}$ is larger than $\mathcal{F}_{\text{Haar}}^{(2)}$. So we can regard the SEA as a better ansatz in the sense that it has better trainability while the expressibility is not sacrificed too much. From the simulation results in Fig. 3, we can see that the second frame potential of the SEA is pretty close to the optimal value.

Numerical Simulation of Experiments.— To verify the advantages of SEA on both efficiency and trainability, we investigate the performance as well as the magnitude of cost gradient of SEA and other ansatzes in estimating the ground state energy of chemistry and physics models by carrying out numerical simulations of experiments. All simulations are performed using the Paddle Quantum [68] toolkit on the PaddlePaddle Deep Learning Platform [69].

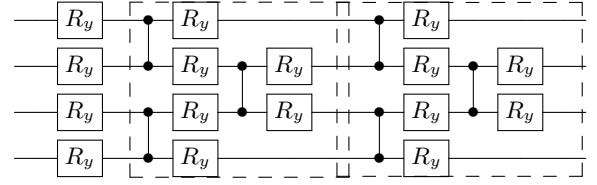


FIG. 4. An example of a 4-qubit ALT with 2 layers. Each layer is composed of the rotation operator gate R_y and control-Z gate.

Applying to chemistry and physics models. To make sure the SEA can meet the aforementioned requirements for VQE, we adopt alternating layered ansatz (ALT) [54], which is a famous class in the hardware-efficient ansatz, for the Schmidt coefficient layer and the LBC layer in the following parts. An example of ALT is shown in Fig. 4.

Here we use 14-qubit dinitrogen (N_2) molecule and the 14-qubit Heisenberg model as examples for numerical simulations of VQE. The structure of SEA is shown in Fig. 2, where U_1 , U_2 , and U_3 are all 7-qubit ALTs with a depth of 30. For different Hamiltonians, we could adjust the K in Proposition 1 to obtain SEAs with different entangling capabilities. Considering that the N_2 molecule and the Heisenberg model we choose are both weakly entangled, we use two kinds of SEA named SEA_2 and SEA_3 to learn these models' ground state energies. To be specific, SEA_2 is the 14-qubit SEA of Schmidt coefficient layer as a 2-qubit ALT and entangling layer as 2 CNOTs, which means a composition of 2 CNOTs controlled and targeted on the qubit-pairs $\{(0, 7), (1, 8)\}$. SEA_3 is the 14-qubit SEA of Schmidt coefficient layer as a 3-qubit ALT and entangling layer as 3 CNOTs, which implement on the qubit-pairs $\{(i, 7+i)\}_{i=0}^2$. As mentioned before, we can also set Schmidt coefficient layer as a subSEA. To verify this point, we use an SEA with Schmidt coefficient layer being the 7-qubit subSEA, which is called SEA_Sch , in our simulations.

For the purpose of studying the advantages of SEA, we compare a 14-qubit SEA with a 14-qubit ALT and a 14-qubit random circuit [45] in the task of VQE with a similar number of parameters by setting different depth for different ansatzes. The specific calculation methods of parameter numbers are given in the Sec.VII of the Supplemental Material. The reason for choosing an ALT and a random circuit is that they both have a strong expressibility and they can be regarded as a 2-design when their depth are large [45, 54]. After setting up the ansatzes, we employ a stochastic gradient descent optimizer to iteratively update parameters for 400 iterations.

The simulation results of N_2 molecule and the Heisenberg model are shown in Fig. 5 and Fig. 6, respectively. Both figures illustrate the efficiency of SEA on VQE. We can observe that with a similar number of parameters, there is a visible gap in the accuracy of estimating the ground energy by different ansatzes. Both SEA_2 and SEA_3 converge rapidly and get an approximate value of ground energy while the results of the ALT and random circuit are hard to be optimized in 400 iterations. Furthermore, it is also valid to replace the three parts of SEA with other structures. The SEA_Sch in Fig. 5 and

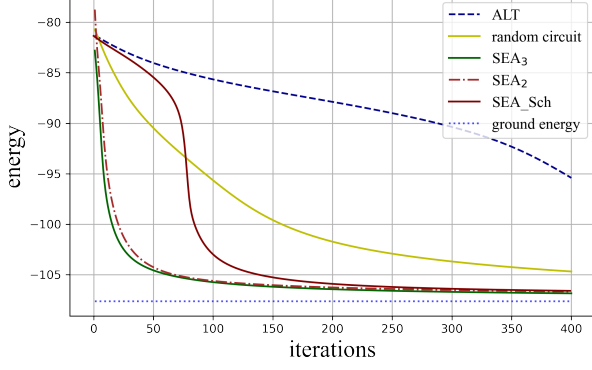


FIG. 5. **Numerical simulations of VQE on N_2 (14-qubit).** The blue dotted line is the theoretical ground energy of N_2 , and the lines from top to bottom represent the experimental results of ALT, the random circuit, SEA of Schmidt coefficient layer as subSEA, SEA with 2 CNOTs, and SEA with 3 CNOTs, respectively. j ($j = 2, 3$) CNOTs means that we set a composition of j CNOTs controlled and targeted on the qubit-pairs $\{(i, N + i)\}_{i=0}^{j-1}$.

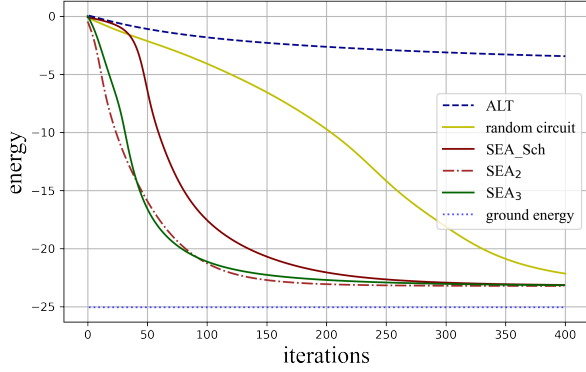


FIG. 6. **Numerical simulations of VQE on Heisenberg model (14-qubit).** The Hamiltonian is chosen to be the 14-qubit 1-dimensional spin-1/2 antiferromagnetic Heisenberg model with periodical boundary condition, i.e., $H = \sum_{i=1}^{14} (X_i X_{i+1} + Y_i Y_{i+1} + Z_i Z_{i+1})$. The blue dotted line is the theoretical ground energy of the Hamiltonian H , and the other lines from top to bottom represent the results of the ALT, random circuit, SEA of Schmidt coefficient layer as subSEA, SEA with 3 CNOTs and SEA with 2 CNOTs, respectively.

Fig. 6 both show that when we choose Schmidt coefficient layer as subSEA, this kind of SEA also has a good performance on VQE like SEA_2 or SEA_3 . In addition to SEA_Sch , the Sec. VII of the Supplemental Material presents the result of SEA whose Schmidt coefficient layer is $R_y(\theta)^{\otimes N}$. We can also see that this kind of SEA has better performance than ALT and random circuit, which further verifies the effectiveness of SEA in practical applications.

From the numerical experiment of VQE, we can see that SEA has an advantage in efficiency. Since we only use 2 or 3

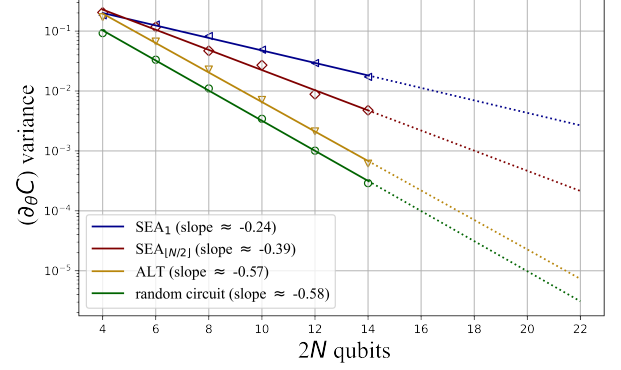


FIG. 7. **Comparison of the scaling of the average variance of gradients between different ansatzes on the Heisenberg model.** This shows the semi-log plot of the average value of the variance of each parameters in the circuit. The depth of each part of SEA is 30 and we ensure different ansatzes have similar numbers of parameters by setting different depth. The solid part of the fitted lines represents the range we experiment with, while the dashed part represents the expected performance on a larger range.

CNOTs and adjust the structure of Schmidt coefficient layer to obtain good results, the experiment results also support Proposition 1.

Gradient experiments. For both experiments on gradients with different numbers of qubits, we consider the 1-dimensional spin-1/2 antiferromagnetic Heisenberg model where the Hamiltonian is $H = \sum_{i=1}^{2N} (X_i X_{i+1} + Y_i Y_{i+1} + Z_i Z_{i+1})$ with periodic boundary condition. We use different ansatzes and calculate the gradient of the cost function $C(\theta) = \langle 0|^{\otimes 2N} U(\theta)^\dagger H U(\theta) |0\rangle^{\otimes 2N}$ with respect to each parameter, where $U(\theta)$ represents the unitary of the ansatz.

We first conduct experiments with the ansatzes used in the previous numerical simulations of VQE. The SEAs we chose are SEA_1 and $SEA_{[N/2]}$, which still adopt ALT as the Schmidt coefficient layer and the LBC layer. For each N , ALT and random circuit with similar numbers of parameters as SEAs are selected for comparison.

The average variances of parameters of different ansatzes are compared in Fig. 7. We also extract the variance of the largest partial derivative in each sample, which is shown in the Sec. VII of the Supplemental Material. It is clearly demonstrated that all these variances decay exponentially as the number of qubits increases. However, the slopes of the red and the blue lines are nearly half of the slopes of the other lines, which means the SEA has a much lower rate of decay of variance.

To better illustrate how our structure increases the scaling of variance, we further inspect the gradient with respect to the parameter in different parts of SEA. As shown in Fig. 8, we look into the gradients with respect to the parameters of the R_y gates in the Schmidt coefficient layer and the LBC layer. As a comparison, we also consider a single parameter R_y gate in the middle of a circuit that forms a 2-design with sufficient depth. The two parts split by the gate are both local

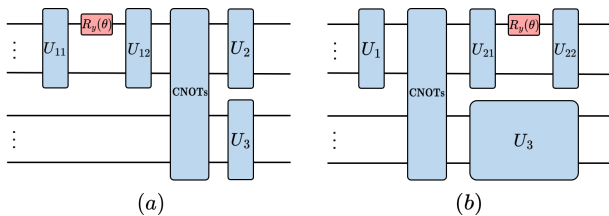


FIG. 8. **The structures of SEA used for studying the scaling of variance of general circuits** Panel (a) shows the R_y gate located in Schmidt coefficient layer. Panel (b) shows the R_y gate located in the LBC layer. Parameter $\theta \in [0, 2\pi)$ is uniformly chosen and $U_1, U_{11}, U_{12}, U_2, U_{21}, U_{22}, U_3$ are Haar randomly chosen from unitary group in each round of sampling. $CNOTs$ is composed by a number of CNOTs.

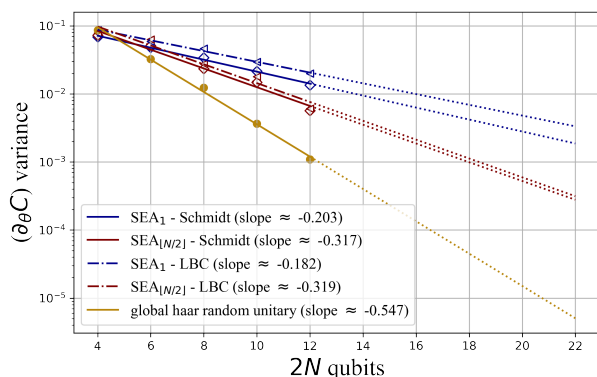


FIG. 9. **Comparison of the scaling of variance between general structure of SEA and general random circuit.** The SEA_1 -Schmidt and the $SEA_{\lfloor N/2 \rfloor}$ -Schmidt show the semi-log plot of the variance of gradient with respect to the parameter in Schmidt coefficient layer. The SEA_1 -LBC and the $SEA_{\lfloor N/2 \rfloor}$ -LBC show the semi-log plot of the variance of gradient with respect to the parameter in LBC layer. The markers on the fitted lines represent the results from our experiments. The dotted part of the lines represents the expected performance on a larger range.

2-designs and are represented by Haar random unitaries in our experiments. Fig. 9 summarizes the results of the variance of parameters located in the Schmidt coefficient layer and the LBC layer, respectively.

From Fig. 9, we see that no matter where this parameter is located in SEA, the variance of its gradient has a decay speed lower than the decay speed of variance of the parameter in a sufficiently random circuit that forms a 2-design. This fact indicates that the variance of SEA has significant improvement compared to using an ansatz that forms a 2-design, indicating an evident mitigation of barren plateaus. It is also worth noting that the fewer CNOTs in the entangling layer,

the larger variance it will have, which is in line with Proposition 3. Specifically, in our experiments, if the scale of the problem is larger than 12 qubits, the variance of the gradients in a 2-design circuit will be less than 10^{-3} . However, this bound of scale can be increased to 18 qubits using SEA with $\lfloor \frac{N}{2} \rfloor$ CNOTs according to our experiment results. With SEA of weaker expressibility, this bound can be further increased. In other words, we can notably increase the scale of problems with the same limited scaling of gradients by using SEA instead of a 2-design circuit. Therefore, SEA is more likely to scale to larger systems on VQE tasks because of its improvement in trainability by mitigating barren plateaus.

Concluding remarks.— The barren plateaus phenomenon that comes with the strong expressibility of an ansatz severely limits the trainability of the VQE. The main contribution of this work is proposing an ansatz structure SEA to mitigate the barren plateaus in optimizing parameterized circuits for quantum dynamics simulations. With the idea of Schmidt decomposition, we invent the SEA by removing the redundant expressibility in universal PQCs. We in particular have provided an explicit construction of SEA that has enough expressibility to generate arbitrary pure quantum states. Moreover, SEA does not form a unitary 2-design, and by tuning the number of CNOT gates, it can efficiently mitigate barren plateaus. From the perspective of frame potential, we prove that SEA has high trainability without losing too much expressibility, which allows a trade-off between trainability and expressibility. Numerical simulations show that SEA can be applied to approximate the ground state of the N_2 molecule and the Heisenberg model, whose numerical results confirm the effectiveness of SEA. We further compare the scaling of variance in partial derivatives between different ansatzes and establish that SEA can obtain a quadratically lower rate of decay of variance, implying that SEA can considerably mitigate the barren plateaus of VQE.

We note that SEA is also effective in principle for other tasks with the sole purpose of generating a pure state, e.g., combinatorial optimization [70] and entanglement detection [71]. It is natural to explore how to extend our structure by considering multipartite systems and other possible designs. We also remark that there are other proposals for dealing with barren plateaus [41, 72–74], and for using meta-learning to improve efficiency [75–78]. The combination between SEA and other approaches such as adaptive methods may be worth a future study. Moreover, with recent works exploiting the symmetry of VQAs [79–81], it is also worth studying how to improve the performance of SEA from this perspective.

Acknowledgements. X. L. and G. L. contributed equally to this work. We would like to thank Runyao Duan, Yin Mo, Chengkai Zhu, and Youle Wang for helpful discussions. Part of this work was done when X. L., G. L., J. H. and H. Z. were interns at Baidu Research.

[1] J. Preskill, arXiv preprint arXiv:1203.5813 (2012).

[2] S. Lloyd, Science **273**, 1073 (1996).

- [3] A. W. Harrow, A. Hassidim, and S. Lloyd, *Physical review letters* **103**, 150502 (2009).
- [4] A. M. Childs and W. van Dam, *Reviews of Modern Physics* **82**, 1 (2010).
- [5] A. Montanaro, *npj Quantum Information* **2**, 15023 (2016).
- [6] J. Preskill, *Quantum* **2**, 79 (2018).
- [7] Y. Cao, J. Romero, J. P. Olson, M. Degroote, P. D. Johnson, M. Kieferová, I. D. Kivlichan, T. Menke, B. Peropadre, N. P. Sawaya, *et al.*, *Chemical reviews* **119**, 10856 (2019).
- [8] S. McArdle, S. Endo, A. Aspuru-Guzik, S. C. Benjamin, and X. Yuan, *Reviews of Modern Physics* **92**, 015003 (2020).
- [9] M. Schuld and F. Petruccione, *Machine Learning with Quantum Computers* (2021).
- [10] J. Biamonte, P. Wittek, N. Pancotti, P. Rebentrost, N. Wiebe, and S. Lloyd, *Nature* **549**, 195 (2017).
- [11] H.-Y. Huang, R. Kueng, G. Torlai, V. V. Albert, and J. Preskill, *arXiv:2106.12627*, 1 (2021), [arXiv:2106.12627](https://arxiv.org/abs/2106.12627).
- [12] S. Jerbi, L. J. Fiderer, H. P. Nautrup, J. M. Kübler, H. J. Briegel, and V. Dunjko, *arXiv:2110.13162*, 1 (2021), [arXiv:2110.13162](https://arxiv.org/abs/2110.13162).
- [13] K. Mitarai, M. Negoro, M. Kitagawa, and K. Fujii, *Physical Review A* **98**, 032309 (2018), [arXiv:1803.00745](https://arxiv.org/abs/1803.00745).
- [14] F. Arute, K. Arya, R. Babbush, D. Bacon, J. C. Bardin, R. Barends, R. Biswas, S. Boixo, F. G. Brandao, D. A. Buell, *et al.*, *Nature* **574**, 505 (2019).
- [15] Y. Wu, W.-S. Bao, S. Cao, F. Chen, M.-C. Chen, X. Chen, T.-H. Chung, H. Deng, Y. Du, D. Fan, M. Gong, C. Guo, C. Guo, S. Guo, L. Han, L. Hong, H.-L. Huang, Y.-H. Huo, L. Li, N. Li, S. Li, Y. Li, F. Liang, C. Lin, J. Lin, H. Qian, D. Qiao, H. Rong, H. Su, L. Sun, L. Wang, S. Wang, D. Wu, Y. Xu, K. Yan, W. Yang, Y. Yang, Y. Ye, J. Yin, C. Ying, J. Yu, C. Zha, C. Zhang, H. Zhang, K. Zhang, Y. Zhang, H. Zhao, Y. Zhao, L. Zhou, Q. Zhu, C.-Y. Lu, C.-Z. Peng, X. Zhu, and J.-W. Pan, *Physical Review Letters* **127**, 180501 (2021).
- [16] H.-S. Zhong, H. Wang, Y.-H. Deng, M.-C. Chen, L.-C. Peng, Y.-H. Luo, J. Qin, D. Wu, X. Ding, Y. Hu, P. Hu, X.-Y. Yang, W.-J. Zhang, H. Li, Y. Li, X. Jiang, L. Gan, G. Yang, L. You, Z. Wang, L. Li, N.-L. Liu, C.-Y. Lu, and J.-W. Pan, *Science* **370**, 1460 (2020).
- [17] H.-S. Zhong, Y.-H. Deng, J. Qin, H. Wang, M.-C. Chen, L.-C. Peng, Y.-H. Luo, D. Wu, S.-Q. Gong, H. Su, *et al.*, *Physical review letters* **127**, 180502 (2021).
- [18] A. Abbas, D. Sutter, C. Zoufal, A. Lucchi, A. Figalli, and S. Woerner, *Nature Computational Science* **1**, 403 (2021), [arXiv:2011.00027](https://arxiv.org/abs/2011.00027).
- [19] L. S. Madsen, F. Laudenbach, M. F. Askarani, F. Rortais, T. Vincent, J. F. Bulmer, F. M. Miatto, L. Neuhaus, L. G. Helt, M. J. Collins, *et al.*, *Nature* **606**, 75 (2022).
- [20] M. Cerezo, A. Arrasmith, R. Babbush, S. C. Benjamin, S. Endo, K. Fujii, J. R. McClean, K. Mitarai, X. Yuan, L. Cincio, *et al.*, *Nature Reviews Physics* **3**, 625 (2021).
- [21] K. Bharti, A. Cervera-Lierta, T. H. Kyaw, T. Haug, S. Alperin-Lea, A. Anand, M. Degroote, H. Heimonen, J. S. Kottmann, T. Menke, W.-K. Mok, S. Sim, L.-C. Kwek, and A. Aspuru-Guzik, *arXiv:2101.08448*, 1 (2021), [arXiv:2101.08448](https://arxiv.org/abs/2101.08448).
- [22] S. Endo, Z. Cai, S. C. Benjamin, and X. Yuan, *arXiv:2011.01382*, 1 (2020), [arXiv:2011.01382](https://arxiv.org/abs/2011.01382).
- [23] A. Peruzzo, J. McClean, P. Shadbolt, M.-H. Yung, X.-Q. Zhou, P. J. Love, A. Aspuru-Guzik, and J. L. O’Brien, *Nature communications* **5**, 4213 (2014).
- [24] J. Romero, J. P. Olson, and A. Aspuru-Guzik, *Quantum Science and Technology* **2**, 045001 (2017), [arXiv:1612.02806](https://arxiv.org/abs/1612.02806).
- [25] X. Wang, Z. Song, and Y. Wang, *Quantum* **5**, 483 (2021), [arXiv:2006.02336](https://arxiv.org/abs/2006.02336).
- [26] I. Cong, S. Choi, and M. D. Lukin, *Nature Physics* **15**, 1273 (2019), [arXiv:1810.03787](https://arxiv.org/abs/1810.03787).
- [27] W. Li and D.-L. Deng, *arXiv:2108.13421* (2021), [arXiv:2108.13421](https://arxiv.org/abs/2108.13421).
- [28] G. Li, Z. Song, and X. Wang, in *Proceedings of the AAAI Conference on Artificial Intelligence*, Vol. 35 (2021) pp. 8357–8365.
- [29] M. C. Caro, H.-Y. Huang, M. Cerezo, K. Sharma, A. Sornborger, L. Cincio, and P. J. Coles, *arXiv:2111.05292*, 1 (2021), [arXiv:2111.05292](https://arxiv.org/abs/2111.05292).
- [30] E. Farhi and H. Neven, *arXiv:1802.06002*, 1 (2018), [arXiv:1802.06002](https://arxiv.org/abs/1802.06002).
- [31] E. Farhi, J. Goldstone, and S. Gutmann, *arXiv preprint arXiv:1411.4028* (2014).
- [32] L. Zhou, S.-T. Wang, S. Choi, H. Pichler, and M. D. Lukin, *Physical Review X* **10**, 021067 (2020), [arXiv:1812.01041](https://arxiv.org/abs/1812.01041).
- [33] M. Benedetti, E. Lloyd, S. Sack, and M. Fiorentini, *Quantum Science and Technology* **4**, 043001 (2019).
- [34] A. Kandala, A. Mezzacapo, K. Temme, M. Takita, M. Brink, J. M. Chow, and J. M. Gambetta, *Nature* **549**, 242 (2017).
- [35] M. R. Hoffmann and J. Simons, *The Journal of chemical physics* **88**, 993 (1988).
- [36] J. Lee, W. J. Huggins, M. Head-Gordon, and K. B. Whaley, *Journal of chemical theory and computation* **15**, 311 (2018).
- [37] H. R. Grimsley, S. E. Economou, E. Barnes, and N. J. Mayhall, *Nature communications* **10**, 1.
- [38] H. L. Tang, V. Shkolnikov, G. S. Barron, H. R. Grimsley, N. J. Mayhall, E. Barnes, and S. E. Economou, *PRX Quantum* **2**, 020310 (2021).
- [39] I. G. Ryabinkin, R. A. Lang, S. N. Genin, and A. F. Izmaylov, “Iterative qubit coupled cluster approach with efficient screening of generators,” (2019), [arXiv:1906.11192](https://arxiv.org/abs/1906.11192) [quant-ph].
- [40] K. Bharti and T. Haug, *Physical Review A* **104**, L050401 (2021).
- [41] H. R. Grimsley, G. S. Barron, E. Barnes, S. E. Economou, and N. J. Mayhall, [arXiv:2204.07179](https://arxiv.org/abs/2204.07179) (2022), [arXiv:2204.07179](https://arxiv.org/abs/2204.07179).
- [42] T. Haug, K. Bharti, and M. S. Kim, *PRX Quantum* **2**, 1 (2021), [arXiv:2102.01659](https://arxiv.org/abs/2102.01659).
- [43] Y. Du, Z. Tu, X. Yuan, and D. Tao, *Physical Review Letters* **128**, 80506 (2022).
- [44] Z. Holmes, K. Sharma, M. Cerezo, and P. J. Coles, *PRX Quantum* **3**, 010313 (2022).
- [45] J. R. McClean, S. Boixo, V. N. Smelyanskiy, R. Babbush, and H. Neven, *Nature communications* **9**, 1 (2018).
- [46] K. Zhang, M.-H. Hsieh, L. Liu, and D. Tao, *arXiv preprint arXiv:2112.15002* (2021).
- [47] H.-K. Zhang, C. Zhu, G. Liu, and X. Wang, [arXiv:2205.05056](https://arxiv.org/abs/2205.05056), 1 (2022), [arXiv:2205.05056](https://arxiv.org/abs/2205.05056).
- [48] S. Sim, P. D. Johnson, and A. Aspuru-Guzik, *Advanced Quantum Technologies* **2**, 1900070 (2019).
- [49] K. Nakaji and N. Yamamoto, *Quantum* **5**, 434 (2021).
- [50] K. Sharma, M. Cerezo, L. Cincio, and P. J. Coles, *Physical Review Letters* **128**, 180505 (2022), [arXiv:2005.12458](https://arxiv.org/abs/2005.12458).
- [51] C. Ortiz Marrero, M. Kieferová, and N. Wiebe, *PRX Quantum* **2**, 040316 (2021), [arXiv:2010.15968](https://arxiv.org/abs/2010.15968).
- [52] E. Grant, L. Wossnig, M. Ostaszewski, and M. Benedetti, *Quantum* **3**, 214 (2019), [arXiv:1903.05076](https://arxiv.org/abs/1903.05076).
- [53] G. Verdon, M. Broughton, J. R. McClean, K. J. Sung, R. Babbush, Z. Jiang, H. Neven, and M. Mohseni, *arXiv:1907.05415*, 1 (2019), [arXiv:1907.05415](https://arxiv.org/abs/1907.05415).
- [54] M. Cerezo, A. Sone, T. Volkoff, L. Cincio, and P. J. Coles, *Nature Communications* **12** (2021), [10.1038/s41467-021-21728-w](https://doi.org/10.1038/s41467-021-21728-w).
- [55] M. Kieferova, O. M. Carlos, and N. Wiebe, *arXiv preprint*

- arXiv:2106.09567 (2021).
- [56] A. Pesah, M. Cerezo, S. Wang, T. Volkoff, A. T. Sornborger, and P. J. Coles, *Physical Review X* **11**, 041011 (2021), [arXiv:2011.02966](#).
 - [57] M. A. Nielsen and I. L. Chuang, *Quantum computation and quantum information* (Cambridge university press, 2010).
 - [58] Y.-Y. Shi, L.-M. Duan, and G. Vidal, *Physical review a* **74**, 022320 (2006).
 - [59] D. Nagaj, E. Farhi, J. Goldstone, P. Shor, and I. Sylvester, *Physical Review B* **77**, 214431 (2008).
 - [60] L. Tagliacozzo, G. Evenbly, and G. Vidal, *Physical Review B* **80**, 235127 (2009).
 - [61] N. Nakatani and G. K.-L. Chan, *The Journal of chemical physics* **138**, 134113 (2013).
 - [62] B. G. Wybourne, (1974).
 - [63] J. Biamonte, *Phys. Rev. A* **103**, L030401 (2021).
 - [64] B. Collins and P. Śniady, *Communications in Mathematical Physics* **264**, 773 (2006), [arXiv:0402073 \[math-ph\]](#).
 - [65] Z. Puchała and J. Miszczyk, *Bulletin of the Polish Academy of Sciences Technical Sciences* **65**, 21 (2017), [arXiv:1109.4244](#).
 - [66] J. Eisert, M. Cramer, and M. B. Plenio, , **1** (2008), [arXiv:0808.3773](#).
 - [67] J. M. Renes, R. Blume-Kohout, A. J. Scott, and C. M. Caves, *Journal of Mathematical Physics* **45**, 2171 (2004).
 - [68] "<https://github.com/paddlepaddle/paddle>," .
 - [69] Y. Ma, D. Yu, T. Wu, and H. Wang, *Frontiers of Data and Computing* **1**, 105 (2019).
 - [70] E. Farhi, J. Goldstone, and S. Gutmann, [arXiv:1411.4028 \(2014\)](#), [arXiv:1411.4028](#).
 - [71] K. Wang, Z. Song, X. Zhao, Z. Wang, and X. Wang, *npj Quantum Information* **8**, 1 (2022).
 - [72] H. L. Tang, V. Shkolnikov, G. S. Barron, H. R. Grimsley, N. J. Mayhall, E. Barnes, and S. E. Economou, *PRX Quantum* **2**, 020310 (2021).
 - [73] A. Skolik, J. R. McClean, M. Mohseni, P. van der Smagt, and M. Leib, *Quantum Machine Intelligence* **3**, 1 (2021).
 - [74] T. Volkoff and P. J. Coles, *Quantum Science and Technology* **6**, 025008 (2021), [arXiv:2005.12200](#).
 - [75] G. Verdon, M. Broughton, J. R. McClean, K. J. Sung, R. Babush, Z. Jiang, H. Neven, and M. Mohseni, *arXiv preprint arXiv:1907.05415* (2019).
 - [76] M. Wilson, R. Stromswold, F. Wudarski, S. Hadfield, N. M. Tubman, and E. G. Rieffel, *Quantum Machine Intelligence* **3**, 1 (2021).
 - [77] T. Stollenwerk and S. Hadfield, *arXiv preprint arXiv:2204.01307* (2022).
 - [78] C. Chen, Z. He, L. Li, S. Zheng, and H. Situ, *arXiv preprint arXiv:2106.06248* (2021).
 - [79] H. Zheng, Z. Li, J. Liu, S. Strelchuk, and R. Kondor, *arXiv preprint arXiv:2112.07611* (2021).
 - [80] J. J. Meyer, M. Mularski, E. Gil-Fuster, A. A. Mele, F. Arzani, A. Wilms, and J. Eisert, *arXiv preprint arXiv:2205.06217* (2022).
 - [81] M. Larocca, F. Sauvage, F. M. Sbahti, G. Verdon, P. J. Coles, and M. Cerezo, *arXiv preprint arXiv:2205.02261* (2022).
 - [82] C. Dankert, R. Cleve, J. Emerson, and E. Livine, *Physical Review A* **80**, 012304 (2009).
 - [83] W. Feit, *The representation theory of finite groups* (Elsevier, 1982).
 - [84] J. Emerson, R. Alicki, and K. Życzkowski, *Journal of Optics B: Quantum and Semiclassical Optics* **7**, S347 (2005).
 - [85] M. Fukuda, R. König, and I. Nechita, *Journal of Physics A: Mathematical and Theoretical* **52**, 1 (2019), [arXiv:1902.08539](#).

Supplemental Material for Mitigating barren plateaus of variational quantum eigensolvers

I. PRELIMINARIES

Here we present some supplemental lemmas and define some notations to be used throughout the proof. We write a target quantum state, which is a pure state to be approximated by a PQC, as $|\phi\rangle$ and let the actual circuit output be $|\psi(\boldsymbol{\theta})\rangle$. We may simply write $|\psi\rangle$ if the circuit parameters $\boldsymbol{\theta}$ are unimportant in the context. Moreover, let $F(|\phi\rangle, |\psi\rangle) = |\langle\psi|\phi\rangle|^2$ be fidelity. Unless otherwise specified, $\{|k\rangle\}_{k=0}^{2^N-1}$ are the N -qubit computational bases. We denote $\widetilde{\text{CNOT}} \equiv \prod_{i=0}^{N-i} \text{CNOT}(i, N+i)$ which is a composition of N CNOTs controlled and targeted on the pair $(i, N+i)$ for all $i = 0, \dots, N-1$. Let \bar{i} be a vector for the binary expansion of i , and therefore \bar{i}_j , where $0 \leq j < \lceil \log i \rceil$, is the j -th leading digit of the expansion.

A. t -design and integration over the unitary group

We firstly recall the definition of a t -design. Assume $\mathcal{U} = \{U_k\}_{k=1}^K$ is a finite of unitary operator on \mathbb{C}^D , and $P_{t,t}(U)$ is a polynomial of degree at most t in the matrix elements of U and at most t in those of U^\dagger . Then, we define that \mathcal{U} is a t -design if for every polynomial $P_{t,t}(U)$ we have

$$\frac{1}{K} \sum_{k=1}^K P_{t,t}(U_k) = \int P_{t,t}(U) d\eta(U), \quad (\text{S1})$$

where the integrals with respect to the Haar measure over the unitary group. Particularly, when $t = 2$, the definition is equivalent to the following definition [82].

Definition S1 $\{U_k\}_{k=1}^K$ forms a unitary 2-design if and only if for any linear operators $C, D, \rho \in L(\mathbb{C}^D)$, we have

$$\frac{1}{K} \sum_{k=1}^K U_k^\dagger C U_k \rho U_k^\dagger D U_k = \int_{\mathcal{U}(d)} U^\dagger C U \rho U^\dagger D U d\eta(U). \quad (\text{S2})$$

Based on this definition, we can know whether a unitary group is a 2-design by comparing the both sides of Eq. (S2). Fortunately, according to the Schur's lemma [83], the RHS of Eq. (S3) has a closed form which is shown in lemma S1. The proof of lemma S1 can be seen in [84].

Lemma S1 Let $\{U_k\}_{k=1}^K$ forms a unitary t -design with $t \geq 2$, for any linear operators $C, D, \rho \in L(\mathbb{C}^D)$. We have

$$\int_{\mathcal{U}(d)} U^\dagger C U \rho U^\dagger D U d\eta(U) = \frac{\text{Tr}[CD] \text{Tr}[\rho]}{d} \frac{I}{d} + \left(\frac{d \text{Tr}[C] \text{Tr}[D] - \text{Tr}[CD]}{d(d^2-1)} \right) (\rho - \text{Tr}[\rho] \frac{I}{d}). \quad (\text{S3})$$

Furthermore, we present the following lemma so that we can solve the problem with bipartite system.

Lemma S2 For any bipartite state ρ_{AB} ($d_A = d_B = d$), and arbitrary linear operators $C, D \in L(\mathbb{C}^{d^2})$, we have

$$\int_{\mathcal{U}(d) \otimes \mathcal{U}(d)} d\eta(U) U^\dagger C U \rho U^\dagger D U = t_0 \rho + t_1 \frac{\rho_A \otimes I_B}{d} + t_2 \frac{I_A \otimes \rho_B}{d} + t_3 I_{AB} \text{Tr}(\rho_{AB}), \quad (\text{S4})$$

where $\rho_A = \text{Tr}_B[\rho_{AB}]$, $\rho_B = \text{Tr}_A[\rho_{AB}]$, and $\{t_j\}_{j=0}^3$ can be computed from the following linear system of equations

$$\text{Tr}(CD) = t_0 d^2 + t_1 d^2 + t_2 d^2 + t_3 d^4, \quad (\text{S5})$$

$$\text{Tr}(C_A D_A) = t_0 d^3 + t_1 d + t_2 d^3 + t_3 d^3, \quad (\text{S6})$$

$$\text{Tr}(C_B D_B) = t_0 d^3 + t_1 d^3 + t_2 d + t_3 d^3, \quad (\text{S7})$$

$$\text{Tr}(C) \text{Tr}(D) = t_0 d^4 + t_1 d^2 + t_2 d^2 + t_3 d^2, \quad (\text{S8})$$

that is,

$$\begin{bmatrix} t_0 \\ t_1 \\ t_2 \\ t_3 \end{bmatrix} = \frac{1}{(d^2-1)^2} \begin{bmatrix} \frac{\text{Tr}[CD]}{d^2} - \frac{\text{Tr}[C_A D_A]}{d} - \frac{\text{Tr}[C_B D_B]}{d} + \text{Tr}[C] \text{Tr}[D] \\ -\text{Tr}[CD] + \frac{\text{Tr}[C_A D_A]}{d} + d \text{Tr}[C_B D_B] - \text{Tr}[C] \text{Tr}[D] \\ -\text{Tr}[CD] + d \text{Tr}[C_A D_A] + \frac{\text{Tr}[C_B D_B]}{d} - \text{Tr}[C] \text{Tr}[D] \\ \text{Tr}[CD] - \frac{\text{Tr}[C_A D_A]}{d} - \frac{\text{Tr}[C_B D_B]}{d} + \frac{\text{Tr}[C] \text{Tr}[D]}{d^2} \end{bmatrix}. \quad (\text{S9})$$

Proof Similar to the proof of Lemma S1, Schur's lemma implies that the LHS of Eq. (S4) has an explicitly expression, which is denoted as follows:

$$\int_{\mathcal{U}(d) \otimes \mathcal{U}(d)} d\eta(U) U^\dagger C U \rho U^\dagger D U = t_0 \rho + t_1 \frac{\rho_A \otimes I_B}{d} + t_2 \frac{I_A \otimes \rho_B}{d} + t_3 I_{AB} \text{Tr}(\rho_{AB}). \quad (\text{S10})$$

For simplicity, we define the following two functions:

$$f^{(1)}(\rho) \equiv t_0 \rho + t_1 \rho_A \otimes I_B / d + t_2 I_A \otimes \rho_B / d + t_3 I_{AB} \text{Tr}(\rho_{AB}), \quad (\text{S11})$$

$$f^{(2)}(\rho) \equiv \int_{\mathcal{U}(d) \otimes \mathcal{U}(d)} d\eta(U) U^\dagger C U \rho U^\dagger D U, \quad (\text{S12})$$

where $f^{(1)} = f^{(2)}$.

Then we only need to consider the coefficients t_0, t_1, t_2, t_3 . To calculate the coefficients, we defined the following four operators:

$$T_1(f) \equiv \sum_{i,j} \langle ij | f(I) | ij \rangle, \quad (\text{S13})$$

$$T_2(f) \equiv \sum_{i,j,k} \langle ik | f(|i\rangle\langle j|_A \otimes I_B) | jk \rangle, \quad (\text{S14})$$

$$T_3(f) \equiv \sum_{i,k,l} \langle ik | f(I_A \otimes |k\rangle\langle l|_B) | il \rangle, \quad (\text{S15})$$

$$T_4(f) \equiv \sum_{i,j,k,l} \langle ij | f(|ij\rangle\langle kl|) | kl \rangle. \quad (\text{S16})$$

For Eq. (S5), we have

$$T_1(f^{(1)}) = t_0 \sum_{i,j} \langle ij | I | ij \rangle + t_1 \sum_{i,j} \langle ij | I_A \otimes I_B | ij \rangle + t_2 \sum_{i,j} \langle ij | I_A \otimes I_B | ij \rangle + t_3 d^4 \quad (\text{S17})$$

$$= t_0 d^2 + t_1 d^2 + t_2 d^2 + t_3 d^4, \quad (\text{S18})$$

$$T_1(f^{(2)}) = \sum_{i,j} \langle ij | \int_{\mathcal{U}(d) \otimes \mathcal{U}(d)} d\eta(U) U^\dagger C U I U^\dagger D U | ij \rangle \quad (\text{S19})$$

$$= \text{Tr}(CD). \quad (\text{S20})$$

Since $T_1(f^{(1)}) = T_1(f^{(2)})$, then $\text{Tr}(CD) = t_0 d^2 + t_1 d^2 + t_2 d^2 + t_3 d^4$.

For Eq. (S7), we have

$$\begin{aligned} T_2(f^{(1)}) &= t_0 \sum_{i,j,k} \langle ik | |i\rangle\langle j| \otimes I_B | jk \rangle + t_1 \sum_{i,j,k} \langle ik | |i\rangle\langle j| \otimes I_B | jk \rangle \\ &\quad + \frac{t_2}{d} \sum_{i,j,k} \langle ik | I_A \otimes \text{Tr}[|i\rangle\langle j|] I_B | jk \rangle + t_3 \sum_{i,j,k} \langle ik | I_{AB} \text{Tr}[|i\rangle\langle j| \otimes I_B] | jk \rangle \end{aligned} \quad (\text{S21})$$

$$= t_0 d^3 + t_1 d^3 + t_2 d + t_3 d^3, \quad (\text{S22})$$

$$T_2(f^{(2)}) = \sum_{i,j,k} \langle ik | \int_{\mathcal{U}(d) \otimes \mathcal{U}(d)} d\eta(U) U^\dagger C U (|i\rangle\langle j|_A \otimes I_B) U^\dagger D U | jk \rangle \quad (\text{S23})$$

$$= \sum_{i,j,k} \int_{\mathcal{U}(d) \otimes \mathcal{U}(d)} d\eta(U) \langle ik | U^\dagger C U (|i\rangle\langle j|_A \otimes I_B) U^\dagger D U | jk \rangle \quad (\text{S24})$$

$$= \text{Tr}(C_B D_B). \quad (\text{S25})$$

Since $T_2(f^{(1)}) = T_2(f^{(2)})$, then $\text{Tr}(C_B D_B) = t_0 d^3 + t_1 d^3 + t_2 d + t_3 d^3$.

Similarly, we have

$$T_3(f^{(1)}) = t_0 d^3 + t_1 d + t_2 d^3 + t_3 d^3, \quad (\text{S26})$$

$$T_3(f^{(2)}) = \text{Tr}(C_A D_A), \quad (\text{S27})$$

$$T_4(f^{(1)}) = t_0 d^4 + t_1 d^2 + t_2 d^2 + t_3 d^2, \quad (\text{S28})$$

$$T_4(f^{(2)}) = \text{Tr}(C) \text{Tr}(D). \quad (\text{S29})$$

$$(\text{S30})$$

Since

$$T_3(f^{(1)}) = T_3(f^{(2)}), \quad (\text{S31})$$

$$T_4(f^{(1)}) = T_4(f^{(2)}), \quad (\text{S32})$$

then

$$\text{Tr}(C_A D_A) = t_0 d^3 + t_1 d + t_2 d^3 + t_3 d^3, \quad (\text{S33})$$

$$\text{Tr}(C) \text{Tr}(D) = t_0 d^4 + t_1 d^2 + t_2 d^2 + t_3 d^2. \quad (\text{S34})$$

Up to now, we have proved Eq. (S5) to Eq. (S8).

Let

$$R = \begin{pmatrix} d^2 & d^2 & d^2 & d^4 \\ d^3 & d^1 & d^3 & d^3 \\ d^3 & d^3 & d^1 & d^3 \\ d^4 & d^2 & d^2 & d^2 \end{pmatrix}. \quad (\text{S35})$$

Then

$$R^{-1} = \frac{1}{(d^2 - 1)^2} \begin{pmatrix} \frac{1}{d^2} & -\frac{1}{d} & -\frac{1}{d} & 1 \\ -1 & \frac{1}{d} & d & -1 \\ -1 & d & \frac{1}{d} & -1 \\ 1 & -\frac{1}{d} & -\frac{1}{d} & \frac{1}{d^2} \end{pmatrix}. \quad (\text{S36})$$

Hence, we have

$$\begin{bmatrix} t_0 \\ t_1 \\ t_2 \\ t_3 \end{bmatrix} = R^{-1} \begin{bmatrix} \text{Tr}(CD) \\ \text{Tr}(C_A D_A) \\ \text{Tr}(C_B D_B) \\ \text{Tr}(C) \text{Tr}(D) \end{bmatrix} = \frac{1}{(d^2 - 1)^2} \begin{bmatrix} \frac{\text{Tr}(CD)}{d^2} - \frac{\text{Tr}(C_A D_A)}{d} - \frac{\text{Tr}(C_B D_B)}{d} + \text{Tr}[C] \text{Tr}[D] \\ -\text{Tr}[CD] + \frac{\text{Tr}(C_A D_A)}{d} + d \text{Tr}[C_B D_B] - \text{Tr}[C] \text{Tr}[D] \\ -\text{Tr}[CD] + d \text{Tr}[C_A D_A] + \frac{\text{Tr}(C_B D_B)}{d} - \text{Tr}[C] \text{Tr}[D] \\ \text{Tr}[CD] - \frac{\text{Tr}(C_A D_A)}{d} - \frac{\text{Tr}(C_B D_B)}{d} + \frac{\text{Tr}[C] \text{Tr}[D]}{d^2} \end{bmatrix}, \quad (\text{S37})$$

$$\begin{bmatrix} t_0 \\ t_1 \\ t_2 \\ t_3 \end{bmatrix} = \frac{1}{(d^2 - 1)^2} \begin{bmatrix} \frac{\text{Tr}(CD)}{d^2} - \frac{\text{Tr}(C_A D_A)}{d} - \frac{\text{Tr}(C_B D_B)}{d} + \text{Tr}[C] \text{Tr}[D] \\ -\text{Tr}[CD] + \frac{\text{Tr}(C_A D_A)}{d} + d \text{Tr}[C_B D_B] - \text{Tr}[C] \text{Tr}[D] \\ -\text{Tr}[CD] + d \text{Tr}[C_A D_A] + \frac{\text{Tr}(C_B D_B)}{d} - \text{Tr}[C] \text{Tr}[D] \\ \text{Tr}[CD] - \frac{\text{Tr}(C_A D_A)}{d} - \frac{\text{Tr}(C_B D_B)}{d} + \frac{\text{Tr}[C] \text{Tr}[D]}{d^2} \end{bmatrix}. \quad (\text{S38})$$

■

II. THE EFFECTIVENESS OF SEA ON VQE

In this section, we present a proof of the effectiveness of SEA on VQE. We first give the Proposition S3 to illustrate that SEA can generate an arbitrary pure state. Then in Proposition S4 we demonstrate that the SEA in Proposition S3 can find the ground state energy of a Hamiltonian, which implies the effectiveness of SEA on VQE.

Proposition S3 *If U_1 can generate an arbitrary N -qubit pure state, then given any $2N$ -qubit pure state $|\phi\rangle$, a $2N$ -qubit SEA can generate $|\phi\rangle$ with a certain set of parameters $\hat{\theta} = \{\theta_1, \theta_2, \theta_3\}$, that is,*

$$S(\hat{\theta})|0\rangle^{\otimes 2N} = |\phi\rangle. \quad (\text{S39})$$

Proof

Beginning with Schmidt decomposition, we can write the target state $|\phi\rangle$ as

$$|\phi\rangle = (\hat{U}_2 \otimes \hat{U}_3) \sum_{k=0}^{2^N-1} \lambda_k |k\rangle_A |k\rangle_B, \quad (\text{S40})$$

where A and B are two N -qubit subsystems, \hat{U}_2 and \hat{U}_3 are two unitary operators acting on these two subsystems, $\{|k\rangle\}_{k=0}^{2^N-1}$ are the N -qubit computational bases, and $\{\lambda_k\}_{k=0}^{2^N-1}$ are Schmidt coefficients.

Because $U_1(\boldsymbol{\theta}_1)$ can generate an arbitrary N -qubit pure state, and $U_2(\boldsymbol{\theta}_2), U_3(\boldsymbol{\theta}_3)$ are universal, we can choose a certain set of parameters $\hat{\boldsymbol{\theta}} = \{\hat{\boldsymbol{\theta}}_1, \hat{\boldsymbol{\theta}}_2, \hat{\boldsymbol{\theta}}_3\}$ such that

$$U_1(\hat{\boldsymbol{\theta}}_1)|0\rangle^{\otimes N} = \sum_{k=0}^{2^N-1} \lambda_k |k\rangle, \quad (\text{S41})$$

$$U_2(\hat{\boldsymbol{\theta}}_2) = \hat{U}_2, \quad (\text{S42})$$

$$U_3(\hat{\boldsymbol{\theta}}_3) = \hat{U}_3. \quad (\text{S43})$$

Combining with V , which is a composition of N CNOTs controlled and targeted on the qubit-pairs $\{(i, N+1)\}_{i=0}^{N-1}$, there has

$$V(U_1(\boldsymbol{\theta}_1) \otimes I)|0\rangle_A^{\otimes N}|0\rangle_B^{\otimes N} = \sum_{k=0}^{2^N-1} \lambda_k V|k\rangle_A|0\rangle_B^{\otimes N} \quad (\text{S44})$$

$$= \sum_{k=0}^{2^N-1} \lambda_k |k\rangle_A |k\rangle_B. \quad (\text{S45})$$

Therefore, we have

$$S(\hat{\boldsymbol{\theta}})|0\rangle^{\otimes 2N} = (U_2(\hat{\boldsymbol{\theta}}_2) \otimes U_3(\hat{\boldsymbol{\theta}}_3))V(U_1(\hat{\boldsymbol{\theta}}_1) \otimes I)|0\rangle^{\otimes N}|0\rangle^{\otimes N} \quad (\text{S46})$$

$$= (\hat{U}_2 \otimes \hat{U}_3) \sum_{k=0}^{2^N-1} \lambda_k |k\rangle_A |k\rangle_B. \quad (\text{S47})$$

$$= |\phi\rangle. \quad (\text{S48})$$

■

Proposition S4 For any $2N$ -qubit Hamiltonian H , it holds that

$$\min_S \langle 0|^{\otimes 2N} S^\dagger H S |0\rangle^{\otimes 2N} = E_0, \quad (\text{S49})$$

where E_0 is the ground state energy of H and the optimization is over all unitaries reachable by SEA with U_1 having universal wavefunction expressibility.

Proof

A given $2N$ -qubit Hamiltonian H can be written as follows according to spectral decomposition:

$$H = \sum_{i=0}^m E_i P_i, \quad (\text{S50})$$

where $\{E_i\}_{i=0}^m$ are eigenvalues of H such that $E_0 < E_1 < \dots < E_m$ and P_i is a projector onto the eigenspace V_i corresponding to the eigenvalue E_i . Then given an arbitrary pure state $|\psi\rangle \in V_0$, we have

$$H|\psi\rangle = E_0|\psi\rangle. \quad (\text{S51})$$

Note that when the optimization is over all unitaries reachable by SEA with U_1 having universal wavefunction expressibility, there exists an S such that $|\psi\rangle = S|0\rangle^{\otimes 2N}$. Therefore,

$$\langle 0|^{\otimes 2N} S^\dagger H S |0\rangle^{\otimes 2N} = \langle \psi|H|\psi\rangle \quad (\text{S52})$$

$$= E_0 \langle \psi | \psi \rangle \quad (\text{S53})$$

$$= E_0. \quad (\text{S54})$$

Since it is trivial that $\min_S \langle 0 |^{\otimes 2N} S^\dagger H S | 0 \rangle^{\otimes 2N} \geq E_0$, we have

$$\min_S \langle 0 |^{\otimes 2N} S^\dagger H S | 0 \rangle^{\otimes 2N} = E_0. \quad (\text{S55})$$

■

III. PROOF OF PROPOSITION 1

In this section, we give a detailed proof of Proposition 1. We first give the following lemma that is used in the proof.

Lemma S5 For any descending sequence $\{x_i\}_{i=1}^n$ ($x_i \geq x_{i+1}$), and any $n \geq N \geq M \geq 1$ ($n, N, M \in \mathbb{Z}$), the following is true:

$$\frac{1}{M} \sum_{i=1}^M x_i \geq \frac{1}{N} \sum_{i=1}^N x_i. \quad (\text{S56})$$

Proof Because $N \geq M \geq 1$ and $x_i \geq x_{i+1}$, we have the following formula:

$$\begin{aligned} & \frac{1}{M} \sum_{i=1}^M x_i - \frac{1}{N} \sum_{i=1}^N x_i \\ &= \frac{1}{M} \sum_{i=1}^M x_i - \left(\frac{1}{N} \sum_{i=1}^M x_i + \frac{1}{N} \sum_{i=M+1}^N x_i \right) \end{aligned} \quad (\text{S57})$$

$$= \left(\frac{1}{M} - \frac{1}{N} \right) \sum_{i=1}^M x_i - \frac{1}{N} \sum_{i=M+1}^N x_i \quad (\text{S58})$$

$$= \frac{1}{N} \left(\frac{N-M}{M} \sum_{i=1}^M x_i - \sum_{i=M+1}^N x_i \right) \quad (\text{S59})$$

$$= \frac{N-M}{N} \left(\frac{1}{M} \sum_{i=1}^M x_i - \frac{1}{N-M} \sum_{i=M+1}^N x_i \right) \quad (\text{S60})$$

$$\geq \frac{N-M}{N} \left(\frac{1}{M} \sum_{i=1}^M x_M - \frac{1}{N-M} \sum_{i=M+1}^N x_{M+1} \right) \quad (\text{because } x_i \geq x_{i+1}) \quad (\text{S61})$$

$$= \frac{N-M}{N} (x_M - x_{M+1}) \quad (\text{S62})$$

$$\geq 0, \quad (\text{S63})$$

thus, we obtain $\frac{1}{M} \sum_{i=1}^M x_i - \frac{1}{N} \sum_{i=1}^N x_i \geq 0$, that is, $\frac{1}{M} \sum_{i=1}^M x_i \geq \frac{1}{N} \sum_{i=1}^N x_i$. ■

Proposition 1 If U_1 can generate any N -qubit pure state that is a superposition of at most K computational basis states, then for any $|\phi\rangle$, there exists an SEA output state $|\psi\rangle$ with $F(|\phi\rangle, |\psi\rangle) \geq \min\{\frac{K}{r}, 1\}$, where $F(|\phi\rangle, |\psi\rangle)$ is the fidelity between $|\phi\rangle$ and $|\psi\rangle$, and r is the Schmidt rank of $|\phi\rangle$.

Proof For any $2N$ -qubit target state $|\phi\rangle = \sum_{k=0}^{r-1} \lambda_k |v_k\rangle_A |v_k\rangle_B$, we explicitly construct an SEA, such that $|\psi\rangle = S(\hat{\theta})|0\rangle^{\otimes 2N}$ and $F(|\phi\rangle, |\psi\rangle) \geq \min\{\frac{K}{r}, 1\}$, where $\hat{\theta} = \{\hat{\theta}_1, \hat{\theta}_2, \hat{\theta}_3\}$ is a certain set of parameters.

Suppose $\{\lambda_k\}_{k=0}^{r-1}$ is the Schmidt coefficients of $|\phi\rangle$ sorted in descending order. Similar to the proof of Proposition S3, we can choose a certain set of parameters $\hat{\theta}$ such that

$$U_1(\hat{\theta}_1)|0\rangle_A^{\otimes N} = \frac{1}{\sqrt{M}} \sum_{k=0}^{\min\{K, r\}-1} \lambda_k |k\rangle, \quad (\text{S64})$$

$$U_2(\hat{\theta}_2)|k\rangle_A = |v_k\rangle_A, \quad (\text{S65})$$

$$U_3(\hat{\theta}_3)|k\rangle_B = |v_k\rangle_B, \quad (\text{S66})$$

where $M = \sum_{k=0}^{\min\{K,r\}-1} \lambda_k^2$. Then

$$|\psi\rangle = S(\hat{\theta})|0\rangle^{\otimes 2N} = \frac{1}{\sqrt{M}} \sum_{k=0}^{\min\{K,r\}-1} \lambda_k |v_k\rangle_A |v_k\rangle_B. \quad (\text{S67})$$

Hence

$$F(|\phi\rangle, |\psi\rangle) = |\langle\phi|\psi\rangle|^2 \quad (\text{S68})$$

$$= \left(\frac{1}{\sqrt{M}} \sum_{k=0}^{\min\{K,r\}-1} \lambda_k^2 \right)^2 \quad (\text{S69})$$

$$= \frac{1}{M} \left(\sum_{k=0}^{\min\{K,r\}-1} \lambda_k^2 \right)^2 \quad (\text{S70})$$

$$= \sum_{k=0}^{\min\{K,r\}-1} \lambda_k^2 \quad (\text{S71})$$

$$\geq \frac{\min\{K,r\}}{r} \sum_{k=0}^{r-1} \lambda_k^2 \quad (\text{due to lemma S5}) \quad (\text{S72})$$

$$= \frac{\min\{K,r\}}{r} \quad (\text{S73})$$

$$= \min\left\{\frac{K}{r}, 1\right\}, \quad (\text{S74})$$

with equality holds if and only if $\lambda_i = \lambda_j, \forall i, j = 0, \dots, r-1$. ■

IV. PROOF OF PROPOSITION 2

Here we prove the Proposition 2 about SEA does not form a 2-design. We first present Lemma S6, which is used in the proof.

Lemma S6 $\widetilde{\text{CNOT}} = \sum_{i=0}^{2^n-1} |i\rangle\langle i|_A \otimes V_{B_i}$, where A, B are subsystems and $V_{B_i} = \bigotimes_{j=0}^{n-1} X_j^{i_j} I_j^{\bar{i}_j}$, $i_j \in \{0, 1\}$, that is the operator on the subsystem B that represents the binary bit of i is 1 acting on pauli X , and 0 acting on I . Then V_{B_i} has the following properties:

1. $[V_{B_i}, V_{B_j}] = 0$;
2. $V_{B_i} = V_{B_i}^\dagger$;
3. $\langle 0|^{\otimes n} V_{B_i} V_{B_j} |0\rangle^{\otimes n} = \delta_{ij}$,

where δ_{ij} is Kronecker delta.

Lemma S6 can be easily proved using properties of Pauli operators.

Proposition 2 SEA with $U_i (i = 1, 2, 3)$ being local 2-design and $\widetilde{\text{CNOT}}$ as entangling layer does not form a 2-design on the global system.

Proof Without losing generality, we only consider the SEA with $2n$ qubits in this proof. Lemma S1 says that if an ansatz forms a 2-design, the Eq. (S3) should hold for any linear operators $C, D, \rho \in L(\mathbb{C}^{d^2})$. Assuming $d = 2^n, C_0 = D_0 = \rho = |0\rangle\langle 0|^{\otimes 2n}$, then if SEA forms a 2-design, we have

$$\int_{U(\theta)} \langle 0|^{\otimes 2n} U^\dagger C_0 U \rho U^\dagger D_0 U |0\rangle^{\otimes 2n} d\eta(U)$$

$$= \int_{\mathcal{U}(d^2)} \langle 0|^{\otimes 2n} U^\dagger C_0 U \rho U^\dagger D_0 U |0\rangle^{\otimes 2n} d\eta(U) \quad (\text{S75})$$

$$= \frac{2}{d^2(d^2+1)}, \quad (\text{S76})$$

where $U(\theta)$ denotes the subset of unitary group generated by SEA, and $d\eta(U)$ denotes the Haar measure.

In the following steps, we will explicitly calculate the Eq. (S75) and prove that it cannot be $\frac{2}{d^2(d^2+1)}$.

For the SEA with $U_i (i = 1, 2, 3)$ being local 2-design and $\widetilde{\text{CNOT}} = V = \sum_{i=0}^{2^n-1} |i\rangle\langle i|_A \otimes V_{B_i}$, the unitary of this ansatz is

$$U = \sum_{i=0}^{2^n-1} (U_2 \otimes U_3) \cdot |i\rangle\langle i| \otimes V_{B_i} \cdot (U_1 \otimes I_B). \quad (\text{S77})$$

Therefore,

$$U|0\rangle^{\otimes 2n} = \sum_{i=0}^{2^n-1} (U_2 \otimes U_3) \cdot |i\rangle\langle i| \otimes V_{B_i} \cdot (U_1 \otimes I_B)|0\rangle^{\otimes 2n}, \quad (\text{S78})$$

$$\langle 0|^{\otimes 2n} U^\dagger = \sum_{i=0}^{2^n-1} \langle 0|^{\otimes 2n} (U_1^\dagger \otimes I_B) \cdot |i\rangle\langle i| \otimes V_{B_i} \cdot (U_2^\dagger \otimes U_3^\dagger). \quad (\text{S79})$$

Then

$$\begin{aligned} & \langle 0|^{\otimes 2n} U^\dagger C_0 U \rho U^\dagger D_0 U |0\rangle^{\otimes 2n} \\ &= \langle 0|^{\otimes 2n} U^\dagger (|0\rangle\langle 0|)^{\otimes 2n} U (|0\rangle\langle 0|)^{\otimes 2n} U^\dagger (|0\rangle\langle 0|)^{\otimes 2n} U |0\rangle^{\otimes 2n} \end{aligned} \quad (\text{S80})$$

$$\begin{aligned} &= \langle 0|^{\otimes 2n} (U_1^\dagger \otimes I_B) \cdot V^\dagger \cdot (U_2^\dagger \otimes U_3^\dagger) (|0\rangle\langle 0|)^{\otimes 2n} (U_2 \otimes U_3) \cdot V \cdot (U_1 \otimes I_B) (|0\rangle\langle 0|)^{\otimes 2n} (U_1 \otimes I_B) \cdot V^\dagger \\ & \quad \cdot (U_2^\dagger \otimes U_3^\dagger) (|0\rangle\langle 0|)^{\otimes 2n} (U_2 \otimes U_3) \cdot V \cdot (U_1 \otimes I_B) |0\rangle^{\otimes 2n} \end{aligned} \quad (\text{S81})$$

$$\begin{aligned} &:= \langle 0|^{\otimes 2n} (U_1^\dagger \otimes I_B) \cdot V^\dagger \cdot (U_2^\dagger \otimes U_3^\dagger) \cdot C_0 \cdot (U_2 \otimes U_3) \cdot \rho_1 \cdot (U_2^\dagger \otimes U_3^\dagger) \cdot D_0 \cdot (U_2 \otimes U_3) \cdot V \\ & \quad \cdot (U_1 \otimes I_B) |0\rangle^{\otimes 2n}, \end{aligned} \quad (\text{S82})$$

where

$$V = \sum_{i=0}^{2^n-1} |i\rangle\langle i|_A \otimes V_{B_i}, \quad (\text{S83})$$

$$\rho_1 = V \cdot (U_1 \otimes I_B) (|0\rangle\langle 0|)^{\otimes 2n} (U_1^\dagger \otimes I_B) \cdot V^\dagger. \quad (\text{S84})$$

Therefore, we have

$$\rho_1^A = \text{Tr}_B[\rho_1] \quad (\text{S85})$$

$$= \sum_{k=0}^{d-1} I_A \otimes \langle k|_B \cdot V \cdot (U_1 \otimes I_B) (|0\rangle\langle 0|)^{\otimes 2n} \cdot (U_1^\dagger \otimes I_B) \cdot V^\dagger \cdot I_A \otimes |k\rangle_B \quad (\text{S86})$$

$$= \sum_{k=0}^{d-1} I_A \otimes \langle k|_B \cdot \left(\sum_{i=0}^{d-1} |i\rangle\langle i|_A \otimes V_{B_i} \right) \cdot (U_1 \otimes I_B) (|0\rangle\langle 0|)^{\otimes 2n} \cdot (U_1^\dagger \otimes I_B) \cdot \left(\sum_{j=0}^{d-1} |j\rangle\langle j|_A \otimes V_{B_j}^\dagger \right) \cdot I_A \otimes |k\rangle_B \quad (\text{S87})$$

$$= \sum_{i,j,k=0}^{d-1} I_A \otimes \langle k|_B \cdot (|i\rangle\langle i|_A \otimes V_{B_i}) \cdot (U_1 \otimes I_B) (|0\rangle\langle 0|)^{\otimes 2n} \cdot (U_1^\dagger \otimes I_B) \cdot (|j\rangle\langle j|_A \otimes V_{B_j}^\dagger) \cdot I_A \otimes |k\rangle_B \quad (\text{S88})$$

$$= \sum_{i,j,k=0}^{d-1} |i\rangle\langle i|_A U_1 (|0\rangle\langle 0|)^{\otimes n} U_1^\dagger |j\rangle\langle j|_A \otimes \langle k|_B V_{B_i} (|0\rangle\langle 0|)^{\otimes n} V_{B_j}^\dagger |k\rangle_B \quad (\text{S89})$$

$$= \sum_{i,j=0}^{d-1} |i\rangle\langle i|_A U_1 (|0\rangle\langle 0|)^{\otimes n} U_1^\dagger |j\rangle\langle j|_A \left(\sum_{k=0}^{d-1} \langle k|_B V_{B_i} (|0\rangle\langle 0|)^{\otimes n} V_{B_j}^\dagger |k\rangle_B \right) \quad (\text{S90})$$

$$= \sum_{i,j=0}^{d-1} |i\rangle\langle i|_A U_1 (|0\rangle\langle 0|)^{\otimes n} U_1^\dagger |j\rangle\langle j|_A \text{Tr}(V_{B_i} (|0\rangle\langle 0|)^{\otimes n} V_{B_j}^\dagger) \quad (\text{S91})$$

$$= \sum_{i,j=0}^{d-1} |i\rangle\langle i|_A U_1 (|0\rangle\langle 0|)^{\otimes n} U_1^\dagger |j\rangle\langle j|_A \text{Tr}(\langle 0|^{\otimes n} V_{B_i} V_{B_j}^\dagger |0\rangle^{\otimes n}) \quad (\text{S92})$$

$$= \sum_{i=0}^{d-1} |i\rangle\langle i| U_1 |0\rangle\langle 0|^{\otimes n} U_1^\dagger |i\rangle\langle i|, \quad (\text{due to lemma S6}) \quad (\text{S93})$$

$$\rho_1^B = \text{Tr}_A[\rho_1] \quad (\text{S94})$$

$$= \sum_{k=0}^{d-1} \langle k|_A \otimes I_B \cdot V \cdot (U_1 \otimes I_B) (|0\rangle\langle 0|)^{\otimes 2n} \cdot (U_1^\dagger \otimes I_B) \cdot V^\dagger \cdot |k\rangle_A \otimes I_B \quad (\text{S95})$$

$$= \sum_{k=0}^{d-1} \langle k|_A \otimes I_B \cdot \left(\sum_{i=0}^{d-1} |i\rangle\langle i|_A \otimes V_{B_i} \right) \cdot (U_1 \otimes I_B) (|0\rangle\langle 0|)^{\otimes 2n} \cdot (U_1^\dagger \otimes I_B) \cdot \left(\sum_{j=0}^{d-1} |j\rangle\langle j|_A \otimes V_{B_j}^\dagger \right) \cdot |k\rangle_A \otimes I_B \quad (\text{S96})$$

$$= \sum_{i,j,k=0}^{d-1} \langle k|_A |i\rangle\langle i|_A U_1 (|0\rangle\langle 0|)^{\otimes n} U_1^\dagger |j\rangle\langle j|_A |k\rangle_A \cdot V_{B_i} (|0\rangle\langle 0|)^{\otimes n} V_{B_j} \quad (\text{S97})$$

$$= \sum_{k=0}^{d-1} \langle k| U_1 |0\rangle\langle 0|^{\otimes n} U_1^\dagger |k\rangle \cdot V_{B_k} |0\rangle\langle 0|^{\otimes n} V_{B_k}. \quad (\text{S98})$$

Then combining lemma S1 and lemma S2, we have

$$\begin{aligned} & \int_{U(\theta)} \langle 0|^{\otimes 2n} U^\dagger C_0 U \rho U^\dagger D_0 U |0\rangle^{\otimes 2n} d\eta(U) \\ &= \int_{U(\theta)} \langle 0|^{\otimes 2n} (U_1^\dagger \otimes I_B) \cdot V^\dagger \cdot (U_2^\dagger \otimes U_3^\dagger) \cdot C_0 \cdot (U_2 \otimes U_3) \cdot \rho_1 \cdot (U_2^\dagger \otimes U_3^\dagger) \cdot D_0 \cdot (U_2 \otimes U_3) \cdot V \\ & \quad \cdot (U_1 \otimes I_B) |0\rangle^{\otimes 2n} \end{aligned} \quad (\text{S99})$$

$$\begin{aligned} &= \int_{\mathcal{U}_1(d)} \langle 0|^{\otimes 2n} (U_1^\dagger \otimes I_B) \cdot V^\dagger \cdot (t_0 \rho_1 + t_1 \frac{\rho_1^A \otimes I_B}{d} + t_2 \frac{I_A \otimes \rho_1^B}{d} + t_3 I_{AB} \text{Tr}(\rho_1)) \cdot V \\ & \quad \cdot (U_1 \otimes I_B) |0\rangle^{\otimes 2n} d\eta(U) \end{aligned} \quad (\text{S100})$$

$$:= M_0 + M_1 + M_2 + M_3, \quad (\text{S101})$$

where

$$M_0 = t_0 \int_{\mathcal{U}_1(d)} \langle 0|^{\otimes 2n} (U_1^\dagger \otimes I_B) \cdot V^\dagger \cdot \rho_1 \cdot V \cdot (U_1 \otimes I_B) |0\rangle^{\otimes 2n} d\eta(U) \quad (\text{S102})$$

$$= t_0, \quad (\text{S103})$$

$$M_1 = \frac{t_1}{d} \int_{\mathcal{U}_1(d)} \langle 0|^{\otimes 2n} (U_1^\dagger \otimes I_B) \cdot V^\dagger \cdot \rho_1^A \otimes I_B \cdot V \cdot (U_1 \otimes I_B) |0\rangle^{\otimes 2n} d\eta(U), \quad (\text{S104})$$

$$M_2 = \frac{t_2}{d} \int_{\mathcal{U}_1(d)} \langle 0|^{\otimes 2n} (U_1^\dagger \otimes I_B) \cdot V^\dagger \cdot I_A \otimes \rho_1^B \cdot V \cdot (U_1 \otimes I_B) |0\rangle^{\otimes 2n} d\eta(U), \quad (\text{S105})$$

$$M_3 = t_3 \int_{\mathcal{U}_1(d)} \langle 0|^{\otimes 2n} (U_1^\dagger \otimes I_B) \cdot V^\dagger \cdot I_{AB} \text{Tr}(\rho_1) \cdot V \cdot (U_1 \otimes I_B) |0\rangle^{\otimes 2n} d\eta(U) \quad (\text{S106})$$

$$= t_3, \quad (\text{S107})$$

$$t_0 = t_3 = \frac{1}{d^2(d+1)^2}, \quad (\text{S108})$$

$$t_1 = t_2 = \frac{1}{d(d+1)^2}. \quad (\text{S109})$$

Now the problem is how do we calculate M_1 and M_2 . Combine with $V = \sum_{i=0}^{d-1} |i\rangle\langle i|_A \otimes V_{B_i}$, there has

$$M_1 = \frac{t_1}{d} \int_{\mathcal{U}_1(d)} \langle 0|^{\otimes 2n} (U_1^\dagger \otimes I_B) \cdot V^\dagger \cdot \rho_1^A \otimes I_B \cdot V \cdot (U_1 \otimes I_B) |0\rangle^{\otimes 2n} d\eta(U) \quad (\text{S110})$$

$$\begin{aligned} &= \frac{t_1}{d} \int_{\mathcal{U}_1(d)} \langle 0|^{\otimes 2n} (U_1^\dagger \otimes I_B) \left(\sum_{i=0}^{d-1} |i\rangle\langle i| \otimes V_{B_i}^\dagger \right) \cdot \left(\sum_{k=0}^{d-1} |k\rangle\langle k| U_1 |0\rangle\langle 0|^{\otimes n} U_1^\dagger |k\rangle\langle k| \otimes I_B \right) \\ &\quad \cdot \left(\sum_{j=0}^{d-1} |j\rangle\langle j| \otimes V_{B_j} \right) (U_1 \otimes I_B) |0\rangle^{\otimes 2n} d\eta(U) \end{aligned} \quad (\text{S111})$$

$$= \frac{t_1}{d} \sum_{i=0}^{d-1} \int_{\mathcal{U}_1(d)} \langle 0|^{\otimes n} U_1^\dagger |i\rangle\langle i| U_1 (|0\rangle\langle 0|)^{\otimes n} U_1^\dagger |i\rangle\langle i| U_1 |0\rangle^{\otimes n} \cdot (\langle 0|0\rangle)^{\otimes n} d\eta(U) \quad (\text{S112})$$

$$= \frac{2t_1}{d(d+1)}, \quad (\text{S113})$$

$$M_2 = \frac{t_2}{d} \int_{\mathcal{U}_1(d)} \langle 0|^{\otimes 2n} (U_1^\dagger \otimes I_B) \cdot V^\dagger \cdot I_A \otimes \rho_1^B \cdot V \cdot (U_1 \otimes I_B) |0\rangle^{\otimes 2n} d\eta(U) \quad (\text{S114})$$

$$\begin{aligned} &= \frac{t_2}{d} \int_{\mathcal{U}_1(d)} \langle 0|^{\otimes 2n} (U_1^\dagger \otimes I_B) \left(\sum_{i=0}^{d-1} |i\rangle\langle i| \otimes V_{B_i}^\dagger \right) \cdot \left(I_A \otimes \sum_{k=0}^{d-1} |k\rangle\langle k| U_1 |0\rangle\langle 0|^{\otimes n} U_1^\dagger |k\rangle\langle k| \otimes V_{B_k} \right) \\ &\quad \cdot \left(\sum_{j=0}^{d-1} |j\rangle\langle j| \otimes V_{B_j} \right) (U_1 \otimes I_B) |0\rangle^{\otimes 2n} d\eta(U) \end{aligned} \quad (\text{S115})$$

$$= \frac{t_2}{d} \sum_{i=0}^{d-1} \int_{\mathcal{U}_1(d)} \langle 0|^{\otimes n} U_1^\dagger |i\rangle\langle i| U_1 (|0\rangle\langle 0|)^{\otimes n} U_1^\dagger |i\rangle\langle i| U_1 |0\rangle^{\otimes n} \cdot (\langle 0|0\rangle)^{\otimes n} d\eta(U) \quad (\text{S116})$$

$$= \frac{2t_2}{d(d+1)}. \quad (\text{S117})$$

Therefore,

$$\text{Eq. (S101)} = M_0 + M_1 + M_2 + M_3 \quad (\text{S118})$$

$$= \frac{2d+6}{d^2(d+1)^3} \quad (\text{S119})$$

$$\neq \frac{2}{d^2(d^2+1)} \quad (n \geq 1, d = 2^n > 1) \quad (\text{S120})$$

$$= \text{Eq. (S76)}. \quad (\text{S121})$$

Thus, SEA with $U_i (i = 1, 2, 3)$ being local 2-design ansatzes and $\widetilde{\text{CNOT}}$ is not a unitary 2-design. \blacksquare

V. PROOF OF PROPOSITION 3

In this section, we present a proof of Proposition 3 by calculating the variance of the cost gradient of the SEA with local 2-designs.

Proposition 3 *For an SEA defined on $2N$ qubits with all sub-blocks being local 2-designs, the variance of the cost gradient scales with the number of qubits as*

$$\text{Var}_{\text{SEA}}[\partial_\mu C] \in \mathcal{O}(2^{-(N+M)}), \quad (\text{S122})$$

where $M \in \{0, 1, \dots, N\}$ denotes the number of CNOT gates used in the entangling layer and the variance is taken over all SEA sub-blocks independently.

Proof Suppose $\mathbf{U} = (U_2 \otimes U_3) \widetilde{\text{CNOT}}(U_1 \otimes I_B)$ is an SEA on a equally bipartite system AB of dimension $d = d_A d_B$ and $d_A = d_B = 2^N$. Note that the $\widetilde{\text{CNOT}}$ in \mathbf{U} represent a collection of M CNOT gates between subsystem A and B . We focus on

a single parameter θ within U_1 such that $U_1 = U_5 (e^{-i\Omega\theta}) U_4$. The case where θ locates at U_2 or U_3 can be analysed similarly. Denote $W = (U_2 \otimes U_3) \widetilde{\text{CNOT}}(U_5 \otimes I_B)$, $V = U_4 \otimes I_B$ and then we have $\mathbf{U} = W (e^{-i\Omega\theta} \otimes I_B) V$. The cost gradient becomes

$$\frac{\partial C}{\partial \theta} = i \text{Tr} \left(V \rho V^\dagger \left[\Omega \otimes I_B, \hat{W}^\dagger H \hat{W} \right] \right), \quad (\text{S123})$$

where $\hat{W} = W (e^{-i\Omega\theta} \otimes I_B)$ and $\hat{U}_5 = U_5 (e^{-i\Omega\theta})$. Suppose all U_i are sampled from local 2-designs. Since the tensor product of two 1-designs is still a 1-design, the expectation of the cost gradient is zero. Then consider the variance

$$\text{Var}_{\text{SEA}} [\partial_\mu C] = -\mathbb{E} \left[\left(\text{Tr} \left(V \rho V^\dagger \left[\Omega \otimes I_B, \hat{W}^\dagger H \hat{W} \right] \right) \right)^2 \right], \quad (\text{S124})$$

where the variance is integrated with respect to U_2, U_3, U_4 and U_5 . We exploit the RTNI package [85] to calculate this integral. It turns out that the exact expression of the variance is dominant by

$$\text{Var}_{\text{SEA}} [\partial_\mu C] \xrightarrow{d \rightarrow \infty} \frac{2 \text{Tr} \left((\text{Tr}_B H)^2 \right) \text{Tr} \left(\Omega^2 \right)}{d_A (d_A^2 - 1)^2 (d_B^2 - 1)} \cdot \left(\begin{array}{c} \left(\begin{array}{ccc} C^t & \rho^t & C^t \\ C & \rho^* & C \end{array} \right) \end{array} \right), \quad (\text{S125})$$

where the last factor is represented by the tensor network notation for convenience and C is $\widetilde{\text{CNOT}}$ for short. The superscript “*” denotes complex conjugate, and the superscript “t” denotes the rearrangement of the indices of $\mathcal{H}_A, \mathcal{H}_B$, i.e.,

$$\left(\begin{array}{c} \mathcal{H}_A \\ \mathcal{H}_B \end{array} \text{---} \begin{array}{|c|} \hline C \\ \hline \end{array} \text{---} \begin{array}{c} \mathcal{H}_A \\ \mathcal{H}_B \end{array} \right), \quad \left(\begin{array}{c} \mathcal{H}_B \\ \mathcal{H}_A \end{array} \text{---} \begin{array}{|c|} \hline C^t \\ \hline \end{array} \text{---} \begin{array}{c} \mathcal{H}_B \\ \mathcal{H}_A \end{array} \right). \quad (\text{S126})$$

Note that a 2-qubit CNOT gate contribute one loop in (S125) and a 2-qubit identity contributes two loops in (S125). Each loop contributes a factor 2. Considering the contributions from $\text{Tr} \left((\text{Tr}_B H)^2 \right) \sim d_A d_B^2$ and $\text{Tr}(\Omega^2) \sim d_A$, the dominant term shall scale with the number of qubits $2N$ as $\mathcal{O}(2^{-(N+M)})$. Note that here we suppose the Hamiltonian H contains terms acting on B trivially, which is reasonable for physical and chemical models with local interactions. Compared to $\mathcal{O}(2^{-2N})$ of the hardware-efficient ansatz forming a global 2-design [45, 54], we find that the SEA could provide a square root advantage on the gradient magnitude with the number of qubits over the hardware-efficient ansatz with sufficient depths, while keeping the accuracy of expressing the low-entangled target states. ■

VI. PROOF OF PROPOSITION 4

In this section we provide a proof of Proposition 4 to estimate the expressibility of SEA, which is quantified by the so-called t -degree frame potential [48], i.e.,

$$\mathcal{F}^{(t)} = \mathbb{E} \left[\left(\text{Tr} \left(\mathbf{U} \rho \mathbf{U}^\dagger \mathbf{V} \rho \mathbf{V}^\dagger \right) \right)^t \right]. \quad (\text{S127})$$

Here $\rho = |0\rangle\langle 0|$ is the zero state on a equally bipartite system AB of dimension $d = d_A d_B$ and $d_A = d_B = 2^N$. The expectation is taken over two copies of the ansatz ensemble $\mathbf{U}, \mathbf{V} \in \mathbb{U}$ independently. For comparison, we first show the results of the Haar measure. For $t = 1$ and $t = 2$, we have

$$\mathcal{F}_{\text{Haar}}^{(1)} = \mathbb{E} \left[\text{Tr} \left(\mathbf{U} \rho \mathbf{U}^\dagger \mathbf{V} \rho \mathbf{V}^\dagger \right) \right] = \frac{\text{Tr}(\rho)}{d} \mathbb{E} \left[\text{Tr} \left(\mathbf{V} \rho \mathbf{V}^\dagger \right) \right] = \frac{(\text{Tr} \rho)^2}{d} = \frac{1}{d}, \quad (\text{S128})$$

$$\mathcal{F}_{\text{Haar}}^{(2)} = \mathbb{E} \left[\left(\text{Tr} \left(\mathbf{U} \rho \mathbf{U}^\dagger \mathbf{V} \rho \mathbf{V}^\dagger \right) \right)^2 \right] \quad (\text{S129})$$

$$= \frac{1}{d^2 - 1} \left[(\text{Tr} \rho)^2 \left((\text{Tr} \rho)^2 - \frac{\text{Tr}(\rho^2)}{d} \right) + \text{Tr}(\rho^2) \left(\text{Tr}(\rho^2) - \frac{(\text{Tr} \rho)^2}{d} \right) \right] \quad (\text{S130})$$

$$= \frac{1}{d^2 - 1} \left((\text{Tr} \rho)^4 + \text{Tr}(\rho^2)^2 - \frac{2(\text{Tr} \rho)^2 \text{Tr}(\rho^2)}{d} \right) = \frac{2}{d(d+1)}. \quad (\text{S131})$$

We can see that the second frame potential is exponentially small in the number of qubits $2N$ with scaling $\mathcal{O}(2^{-4N})$.

Proposition 4 For an SEA defined on $2N$ qubits with all sub-blocks being local 2-designs, the first and second frame potential satisfies

$$\mathcal{F}_{\text{SEA}}^{(1)} = 2^{-2N}, \quad (\text{S132})$$

$$\mathcal{F}_{\text{SEA}}^{(2)} \in \mathcal{O}(2^{-4N}). \quad (\text{S133})$$

Proof For SEAs with sub-blocks being local 2-designs, the 1-degree frame potential is

$$\mathcal{F}_{\text{SEA}}^{(1)} = \mathbb{E} [\text{Tr} (\mathbf{U} \rho \mathbf{U}^\dagger \mathbf{V} \rho \mathbf{V}^\dagger)] \quad (\text{S134})$$

$$= \mathbb{E} \left[\text{Tr} \left((U_2 \otimes U_3) \text{CNOT}(U_1 \otimes I_B) \rho (U_1^\dagger \otimes I_B) \text{CNOT}(U_2^\dagger \otimes U_3^\dagger) \right. \right. \\ \left. \left. (V_2 \otimes V_3) \text{CNOT}(V_1 \otimes I_B) \rho (V_1^\dagger \otimes I_B) \text{CNOT}(V_2^\dagger \otimes V_3^\dagger) \right) \right] \quad (\text{S135})$$

$$= \mathbb{E} \left[\text{Tr} \left((U_2 \otimes U_3) \text{CNOT}(U_1 \otimes I_B) \rho (U_1^\dagger \otimes I_B) \text{CNOT}(U_2^\dagger \otimes U_3^\dagger) \right. \right. \\ \left. \left. \text{CNOT}(V_1 \otimes I_B) \rho (V_1^\dagger \otimes I_B) \text{CNOT} \right) \right], \quad (\text{S136})$$

where we have used the unitary invariance of the Haar measure to eliminate V_2 and V_3 . Integrating with respect to V_1, U_1 , and then U_2, U_3 leads to

$$\mathcal{F}_{\text{SEA}}^{(1)} = \frac{1}{d_A^2} \mathbb{E} \left[\text{Tr} \left((U_2 \otimes U_3) \text{CNOT}(I_A \otimes \text{Tr}_A(\rho)) \text{CNOT}(U_2^\dagger \otimes U_3^\dagger) \right. \right. \\ \left. \left. \text{CNOT}(I_A \otimes \text{Tr}_A(\rho)) \text{CNOT} \right) \right] \quad (\text{S137})$$

$$= \frac{1}{d_A^3 d_B} (\text{Tr} (\text{CNOT}(I_A \otimes \text{Tr}_A(\rho)) \text{CNOT}))^2 = \frac{1}{d_A d_B} = \frac{1}{d}. \quad (\text{S138})$$

That is to say, the 1-degree frame potential of SEA with local 2-designs is optimal, which can be easily seen from the fact that SEA with local 2-designs is an exact 1-design. The second frame potential $\mathcal{F}^{(2)}$ can be calculated similarly. Similar with the proof in the last section, we again exploit the RTNI package [85] to calculate this integral. It turns out that the exact expression of $\mathcal{F}_{\text{SEA}}^{(2)}$ with full CNOTs is also dominant by

$$\mathcal{F}_{\text{SEA}}^{(2)} \xrightarrow{d \rightarrow \infty} \frac{2}{(d_A^2 - 1)^3 (d_B^2 - 1)} \cdot \left(\left(\begin{array}{c} \text{C}^t \\ \text{C} \end{array} \right) \right)^4 = \frac{2d_A^4}{(d_A^2 - 1)^3 (d_B^2 - 1)}, \quad (\text{S139})$$

of scaling $\mathcal{O}(2^{-4N})$, which has no difference with the Haar case in the sense of scaling, though the exact value is larger. ■

This can be easily understood if we replace CNOT gates with identities as the tensor product ansatzes (TEN) in [49], which is easier to compute compactly. Specifically, suppose the number of qubits $2N$ is divisible by k so that the $2N$ qubits could be divided equally into k subsystems with $2N/k$ qubits. The tensor product ansatz is defined by $\mathbf{U} = \bigotimes_{i=1}^k U_i$ with each unitary U_i acting on each subsystem. If the ensembles of U_i are all unitary 2-designs, then the following equality hold

$$\mathcal{F}_{\text{TEN}}^{(2)} = 2^{k-1} \cdot \frac{2^{2N} + 1}{(2^{2N/k} + 1)^k} \cdot \mathcal{F}_{\text{Haar}}^{(2)}. \quad (\text{S140})$$

For large $2N$ and fixed k , we have $\mathcal{F}_{\text{TEN}}^{(2)} \approx 2^{k-1} \mathcal{F}_{\text{Haar}}^{(2)}$ which means that there is no difference in the sense of scaling between the finite tensor product ensemble and the Haar ensemble. They both behave as $\mathcal{O}(2^{-4N})$. This partially explains why the second frame potential of the SEA can have the same scaling as the extreme one.

VII. SUPPLEMENTARY DESCRIPTION OF EXPERIMENTS

In this section, we present results from supplementary numerical experiments. Table S1 shows the specific calculation method for the numbers of parameters. Fig. S1 displays the results of VQE using the SEA of Schmidt coefficient layer as $R_y(\theta)^{\otimes 6}$, entangling layer as 6 CNOTs and the LBC layers as two 6-qubit ALTs. Fig. S2 shows the variance of the largest partial derivative in each sample.

TABLE S1. Comparison of the number of parameters in different ansatzes. N represents the half of qubit number, $l_i (i = 1, 2, 3)$ is the number of layer of U_i .

	SEA	ALT	Random
parameter number	$3N + 6(N - 1)l_1$	$2N + 2(2N - 1)l_2$	$2Nl_3$

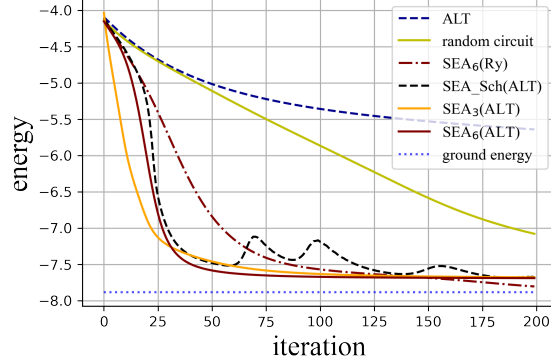


FIG. S1. **Numerical experiment of VQE on LiH (12-qubit).** The blue dotted line is the theoretical ground energy of LiH, and the lines from top to bottom represent the experimental results of ALT, the random circuit, SEA with $R_{ij}(\theta)$ as U_1 and two ALTs as U_2, U_3 and 6 CNOTs as entangling layer, SEA of Schmidt coefficient layer as subSEA, SEA with three ALTs as $U_i (i = 1, 2, 3)$ and 3 CNOTs as entangling layer, SEA with three ALTs as $U_i (i = 1, 2, 3)$ and 6 CNOTs as entangling layer, respectively. $j (j = 3, 6)$ CNOTs means that we set a composition of j CNOTs controlled and targeted on the qubit-pairs $\{(i, N + i)\}_{i=0}^{j-1}$.

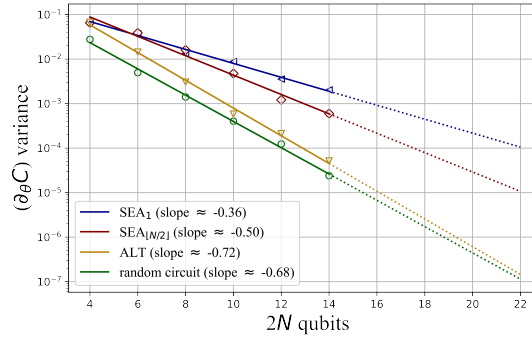


FIG. S2. **Comparison of the scaling of variance between different ansatzes on the Heisenberg model.** It shows the semi-log plot of the variance of the largest partial derivative among parameters in each round of sampling. We ensure different ansatzes have similar number of parameters by setting different depth. The solid part of the fitted lines represents the range we experimented with, while the dotted part represents the expected performance on a larger range.